2013

Epidemic models on adaptive networks with network structure constraints

Ilker Tunc
College of William & Mary - Arts & Sciences

Epidemic models on adaptive networks with network structure constraints

Ilker Tunc

Samsun, Turkey

Master of Science, The College of William and Mary, 2010
Master of Science, Istanbul Technical University, 2006
Bachelor of Science, Middle East Technical University, 2000

A Dissertation presented to the Graduate Faculty
of the College of William and Mary in Candidacy for the Degree of
Doctor of Philosophy

Department of Applied Science

The College of William and Mary
May 2013

APPROVAL PAGE

This Dissertation is submitted in partial fulfillment of
the requirements for the degree of

Doctor of Philosophy

Ilker Tunc

Approved by the Committee, March, 2013

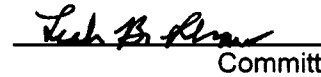

Committee Chair
Associate Professor Leah B. Shaw, Applied Science
The College of William & Mary

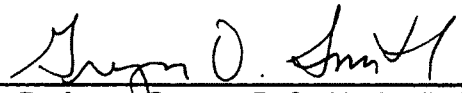

Associate Professor Gregory D. Smith, Applied Science
The College of William & Mary

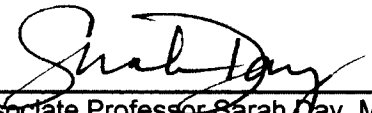

Associate Professor Sarah Day, Mathematics
The College of William & Mary

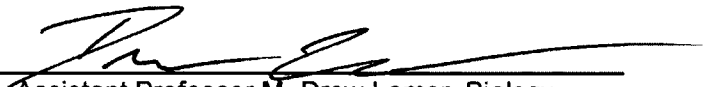

Assistant Professor M. Drew Lamar, Biology
The College of William & Mary

ABSTRACT

Spread of infectious diseases progresses as a result of contacts between the individuals in a population. Therefore, it is crucial to gain insight into the pattern of connections to better understand and possibly control the spread of infectious diseases. Moreover, people may respond to an epidemic by changing their social behaviors to prevent infection. As a result, the structure of the network of social contacts evolves adaptively as a function of the disease status of the nodes. Recently, the dynamic relationships between different network topologies and adaptation mechanisms have attracted great attention in modeling epidemic spread. However, in most of these models, the original network structure is not preserved due to the adaptation mechanisms involving random changes in the links. In this dissertation, we study more realistic models with network structure constraints to retain aspects of the original network structure.

We study a susceptible-infected-susceptible (SIS) disease model on an adaptive network with two communities. Different levels of heterogeneity in terms of average connectivity and connection strength are considered. We study the effects of a disease avoidance adaptation mechanism based on the rewiring of susceptible-infected links through which the disease could spread. We choose the rewiring rules so that the network structure with two communities would be preserved when the rewiring links occur uniformly. The high dimensional network system is approximated with a lower dimensional mean field description based on a moment closure approximation. Good agreement between the solutions of the mean field equations and the results of the simulations are obtained at the steady state. In contrast to the non-adaptive case, similar infection levels in both of the communities are observed even when they are weakly coupled. We show that the adaptation mechanism tends to bring both the infection level and the average degree of the communities closer to each other.

In this rewiring mechanism, the local neighborhood of a node changes and is never restored to its previous state. However, in real life people tend to preserve their neighborhood of friends. We propose a more realistic adaptation mechanism, where susceptible nodes temporarily deactivate their links to infected neighbors and reactivate the links to those neighbors after they recover. Although the original network is static, the subnetwork of active links is evolving.

We drive mean field equations that predict the behavior of the system at the steady state. Two different regimes are observed. In the slow network dynamics regime, the adaptation simply reduces the effective average degree of the network. However, in the fast network dynamics regime, the adaptation further suppresses the infection level by reducing the dangerous links. In addition, non-monotonic dependence of the active degree on the deactivation rate is observed.

We extend the temporary deactivation adaptation mechanism to a scale-free network, where the degree distribution shows heavy tails. It is observed that the tail of the degree distribution of the active subnetwork has a different exponent than that of the original network. We present a heuristic explanation supporting that observation. We derive improved mean field equations based on a new moment closure approximation which is derived by considering the active degree distribution conditioned on the total degree. These improved mean field equations show better agreement with the simulation results than standard mean field analysis based on homogeneity assumptions.

TABLE OF CONTENTS

ACKNOWLEDGEMENTS

First of all, I would like to acknowledge my advisor Leah Shaw. This dissertation would not have been possible without her friendly guidance and her persistent help throughout my doctoral education. Also, I would like to thank to our former post doctoral research associate Maxim S. Shkarayev for his great contributions to this dissertation. I would like to thank to members of my graduate committee for their time, attention and thoughtful comments. I would like to thank to Shadrack Antwi and Yunhan Long for their friendship. Finally, I would like to thank to my wife, my daughter and my son for their love, support and understanding during the long years of my education.

This work was supported by the Army Research Office, Air Force Office of Scientific Research, and by Award Number R01GM090204 from the National Institute of General Medical Sciences. The content is solely the responsibility of the authors and does not necessarily represent the official views of the National Institute of General Medical Sciences or the National Institutes of Health.

Chapter 1

Introduction

The pattern of connections between the individuals in a population affects the dynamics of the disease spreading. Moreover, the structure of the population may change due to infection. In early compartmental models [1, 2], the population is assumed to be homogeneously mixed, where each individual has a chance to contact any other. In this unrealistic assumption, the effect of local connections is neglected. By relaxing the homogenous mixing assumption, recently complex networks [3, 4, 5, 6] have been used in mathematical modeling of epidemic spread. In these models, the structure of the population is modeled as a network, where the nodes represent the individuals and the links represent the relationships between the individuals. In the case where the disease dynamics is fast relative to changes in network connections, the topology of the network can be assumed to be fixed, which is called a static network. However, people may change their social behaviors in response to infection [7, 8, 9]. For example, healthy individuals may reduce the strength of their links with infecteds by hand washing or mask wearing [10], which may alter the subsequent spread of infection, i.e., the state of the nodes. Therefore, a dynamic interaction between the geometry of the network and the state of the nodes occurs. If the network structure evolves as a function of the state of the nodes, then such networks are called as adaptive networks [8]. Various types of adaptation mechanisms have been studied previously. One of them is the rewiring adaptation mechanism [7] based on removing potentially dangerous

links between the susceptible and infected nodes in order to avoid risk of infection. The rules of rewiring process may change depending on how the links to be rewired are chosen. For example, in [7, 11, 12, 13] a susceptible node rewires to a randomly chosen susceptible node, whereas in [14] a susceptible node rewires to a randomly chosen node independent of the infection status. Also, infected nodes may be allowed to rewire [15]. In these models, while the links rewire, the total number of links in the network is kept constant. This might be a valid assumption in the sense that a certain connectivity in the network needs to exist in order to maintain the functionality of the society. In this dissertation, we study how the epidemic spread evolves on adaptive networks with additional network structures under more realistic adaptation strategies.

The topology of the network can be characterized by using various features. One of the most important features of a social network is the community structure [16]. A community is a group of nodes having denser connections within the group than to the rest of the network. In Chapter 2, we study avoidance rewiring in an adaptive network with two heterogeneous communities connected to each other. We study how epidemic evolves in this specific topology and how epidemic spread shapes the network topology.

In real life, we expect that people tend to preserve their original neighborhood even if they change their social contacts to prevent from infection. In the previous models with rewiring adaptation [7, 11, 14, 15], the original neighborhood of the nodes evolves in time. In Chapter 3, we introduce an adaptation mechanism where susceptible nodes temporarily deactivate their links to infected neighbors and reactivate when their neighbors are recovered. We study the effects of this adaptation mechanism on the epidemic spread and investigate how it changes the topology of the network. In Chapter 4, we extend the temporary deactivation/reactivation adaptation model to a scale-free network and study how the degree distribution of the active subnetwork is affected due to infection spreading.

In Section 1.1, we summarize susceptible-infected-susceptible (SIS) model of disease dynamics in a well-mixed system with continuous variables. In Section 1.2, we define some terms related to complex networks used in the later chapters of the dissertation. Finally, in

Section 1.3, we explain SIS dynamics on adaptive networks and show new analytical results which are referenced in Chapter 2 and 3.

1.1 Compartmental SIS model

In mathematical modeling of infectious diseases, often the population is categorized into different compartments depending on the disease status of the individuals [1, 2]. In a susceptible-infected-susceptible (SIS) model, individuals can be in one of the two states: a susceptible (S) who has no immunity to the disease and might become infected as a result of contact with an infectious individual, or an infected (I) who is infected/infectious and can transmit the disease to a susceptible. In this model, infecteds become susceptible again immediately after recovery; infected individuals do not develop immunity to the disease.

Let N_S and N_I denote the number of susceptible and infected individuals, respectively. It is assumed that:

- The rate of new infections is proportional to the number of contacts between susceptible and infected individuals.
- Every individual has the same probability to contact any other; therefore, the number of contacts between the susceptible and infected individuals is proportional to $N_S N_I$ (homogeneous mixing).
- Infecteds have a constant rate of recovery.

Let $N = N_S + N_I$ be constant. For large N, we can treat N_S and N_I as continuous variables and obtain differential equations as follows,

$$\frac{dN_S}{dt} = -\beta N_S N_I + r N_I, \tag{1.1a}$$

$$\frac{dN_I}{dt} = \beta N_S N_I - r N_I. \tag{1.1b}$$

where β is the transmission rate (per capita) and r is the recovery rate. Since N is constant,

we can eliminate one of the variables and reduce the system to one equation,

$$\begin{aligned}\frac{dN_{\mathrm{I}}}{dt} &= f(N_{\mathrm{I}}) \\ &= \beta(N - N_{\mathrm{I}})N_{\mathrm{I}} - rN_{\mathrm{I}}\end{aligned} \tag{1.2}$$

Eq. (1.2) has 2 equilibrium points: the disease-free state $(N_{\mathrm{S}}, N_{\mathrm{I}}) = (N, 0)$ and the endemic state $(N_{\mathrm{S}}, N_{\mathrm{I}}) = (\frac{r}{\beta}, N - \frac{r}{\beta})$. By checking the derivative of $f(N_{\mathrm{I}})$ at these values, we conclude that the disease-free state is stable if $R_0 = \frac{N\beta}{r} < 1$ and unstable if $R_0 = \frac{N\beta}{r} > 1$. R_0 is called the basic reproduction number [1], defined as the average number of secondary infections when an infected individual is introduced into a population with susceptibles. $R_0 = 1$ is the epidemic threshold, determining whether there will be an epidemic or not.

1.2 Basic concepts in complex networks

In mathematical terms, a network can be defined as a graph $G = (V, E)$, where V is the set of *nodes* (vertices) and E is the set of *links* (edges) [17]. Two nodes are called *neighbors* if they are connected with a link. The *degree* (connectivity) of a node is the total number of neighbors of that node. The *degree distribution* of a network, $P(k)$, is defined as the fraction of nodes having degree k or can be defined as the probability that a randomly chosen node has degree k.

Many phenomena around us can be modeled as a complex network. Various kinds of networks appear in different fields of science, such as the world wide web in computing; neural networks, food webs and metabolic networks in biology; citation networks as examples of social systems; and power grids as technological networks.

The specific pattern of connections describes the topology of a network. Simpler network topologies include lattices and random graphs. The structure of the network in these simple models is regular or approximately homogeneous and the mechanism of link formation is simple. However, the structure of real complex networks is generally not regular. There are some common local and global features which are used to understand the topology

of a network. For example the degree distribution is one of the most basic topological characterizations of a network that determines its geometry [17].

An important feature of social networks is community structure. It is widely assumed that social networks show community structure [4]. A community is a group of nodes where denser connectivity is observed within the group compared to outside the group. We can easily observe communities in various networks, such as communities depending on age, sex, location or interests in social networks; functional groupings in metabolic networks; or papers in the same area of research in citation networks.

1.2.1 Erdős-Rényi random networks

One of the simplest network models is the Erdős-Rényi (ER) random graph [18]. In an ER random graph, the links are created randomly between two randomly chosen nodes with a fixed probability p. Let N be the total number of nodes and K be the total number of links. Then, discarding self links and multiple links, the maximum number of links is $\binom{N}{2} = \frac{N(N-1)}{2}$ and $\binom{\frac{N(N-1)}{2}}{K}$ is the number of all possible ER random networks with N nodes and K links. Any ER random network with N nodes and K links is equally probable to be chosen from this ensemble of graphs. In such a random graph, the probability p that a link exists between two randomly chosen nodes can be found as follows,

$$\binom{N}{2}p = K \quad \Rightarrow \quad p = \frac{2K}{N(N-1)}$$

Let X denote the random variable that defines the degree of a randomly chosen node. Let $P(k) \equiv P(X = k)$ denote the probability that a randomly chosen node has degree k. Then,

$$P(k) = \binom{N-1}{k} p^k (1-p)^{N-1-k} \quad k = 0, \ldots, N-1$$

where

$$\sum_{k=0}^{N-1} P(k) = 1$$

The average degree of a node is

$$\kappa = E(X) = \sum_{k=0}^{N-1} kP(k) = p(N-1) = \frac{2K}{N} \tag{1.3}$$

In a finite ER random graph, the degree distribution is binomial. In the limit of $N \to \infty$ and $p \to 0$ while keeping the average degree κ fixed, the binomial distribution can be approximated by the Poisson distribution,

$$P(k) = e^{-\kappa}\frac{\kappa^k}{k!}$$

where the average degree is $E(X) = \kappa$ and the variance in degree is $V(X) = \kappa$.

1.2.2 Scale-free networks

The degree distribution of the most of real networks does not follow the Poisson distribution. Many real-world networks display power-law scaling in the tail of the degree distribution [19], such as the world wide web [20], the internet [21] and metabolic networks [22]. Such networks with power-law degree distribution are called scale-free networks [19]. The typical value of the exponent γ of the degree distribution, $P(k) \sim k^{-\gamma}$, ranges between $2 \leq \gamma \leq 3$. In these networks, there are a few nodes (hubs) with many neighbors and a large number of poorly connected nodes. There are various algorithms to generate a scale-free network. Particularly, in Chapter 4, we used the Barabási-Albert algorithm to generate the network. In the Barabási-Albert (BA) model of a growing network, new nodes make connections with m existing nodes, where m is the minimum number of connection of the nodes [23]. In that model, the new nodes prefer to connect to the nodes with higher degree. As a result of this process, the degree distribution is given by $P(k) = 2m/k^{-3}$ at the steady state. The average degree of the network, $\langle k \rangle = 2m$, is defined and bounded. However, the second moment of the degree distribution is divergent in the limit of infinite network size.

1.3 The SIS model on adaptive networks

In classical compartmental models, it is assumed that the population is homogeneously mixed, where any individual has a chance to contact any other. The local nature of the population is ignored in these models. However, in reality, people have contact with a limited number of individuals. In order to relax that assumption and account for the structure of the population, the population is modeled as a network, where the nodes represent the individuals and the links represent relationships between the individuals.

Moreover, during an epidemic, people might change their social behaviors to avoid exposure to a disease [9]. In a dynamic network, the pattern of connections evolves in time, which affects the dynamics on the network, i.e., the dynamics of the nodes. Moreover, if the links change as a function of the state of the nodes, then a feedback loop is created [8], where both dynamics of the network and the dynamics on the network co-evolve in time depending on each other. Such networks are called adaptive networks [8].

An SIS model on adaptive models was introduced in [7]. In that model disease dynamics is as follows: susceptible nodes become infected with infection rate p per SI link and infected nodes recover with rate r. As an adaptation strategy to avoid infection, susceptible nodes are allowed to remove their links to infected neighbors and rewire to a randomly chosen susceptible node with rewiring rate w.

To analyze the system, it is approximated with a lower dimensional approach, where only the number of nodes and links in various states are considered as state variables. Let N_{S} and N_{I} denote the number of susceptible and infected nodes, respectively. N_{SS}, N_{SI} and N_{II} represent the number of SS, SI and II type links, respectively. In the limit of large N ($N = N_{\mathrm{S}} + N_{\mathrm{I}}$), we can treat the state variables as continuous and derive ordinary differential equations for the time evolution of the nodes,

$$\frac{dN_{\mathrm{S}}}{dt} = rN_{\mathrm{I}} - pN_{\mathrm{SI}}, \tag{1.4a}$$

$$\frac{dN_{\mathrm{I}}}{dt} = -rN_{\mathrm{I}} + pN_{\mathrm{SI}}, \tag{1.4b}$$

and for the links,

$$\frac{dN_{\mathrm{SS}}}{dt} = (r+w)N_{\mathrm{SI}} - pN_{\mathrm{SSI}}, \tag{1.5a}$$

$$\frac{dN_{\mathrm{SI}}}{dt} = 2rN_{\mathrm{II}} + p(N_{\mathrm{SSI}} - N_{\mathrm{ISI}}) - (p+r+w)N_{\mathrm{SI}}, \tag{1.5b}$$

$$\frac{dN_{\mathrm{II}}}{dt} = -2rN_{\mathrm{II}} + pN_{\mathrm{ISI}} + pN_{\mathrm{SI}}, \tag{1.5c}$$

The notation N_{SSI} and N_{ISI} are the expected number of connected triples of nodes of type SSI and ISI, respectively. Equations (1.4) reflect the transitions of nodes between susceptible and infected states, while Eqs. (1.5) reflect the link transitions. For example, in Eq. (1.5a), SI type links become SS links, if the infected node recovers with rate r or if the susceptible node rewires to another susceptible node with rate w. In addition, when a susceptible node gets infected through an SI link, all the SS links associated with that S node would be affected and become SI links with rate p, which is the second term in Eq. (1.5a). Therefore, we need to consider higher order (triple) terms to take this into account. As a result, the system of equations (1.4) and (1.5) is open since it contains unknown quantities corresponding to the statistics of the higher order node formations. To close the system, we approximate the number of triples in the system using the moment closure approximation discussed in [24, 7, 25]:

$$N_{\mathrm{SSI}} = \frac{2N_{\mathrm{SS}}}{N_{\mathrm{S}}}\frac{N_{\mathrm{SI}}}{N_{\mathrm{S}}}N_{\mathrm{S}} \tag{1.6a}$$

$$N_{\mathrm{ISI}} = \left[\frac{N_{\mathrm{SI}}}{N_{\mathrm{S}}}\right]^2 N_{\mathrm{S}} \tag{1.6b}$$

Equation (1.6a) is based on the assumption that, in the neighborhood of an S node, the infected and susceptible neighbors are homogeneously distributed. So, the number of SSI triples is equal to the average number of S neighbors per S node ($\frac{2N_{SS}}{N_S}$) times the average number of I neighbors per S node ($\frac{N_{SI}}{N_S}$) times the total number of S nodes (N_S). In Eq. (1.6b), it is assumed that the distribution of I neighbors of an S node is a Poisson distribution [25].

Node probabilities can be defined as

$$P_S = \frac{N_S}{N} \quad \text{and} \quad P_I = \frac{N_I}{N}, \tag{1.7a}$$

and link probabilities as

$$P_{SS} = \frac{N_{SS}}{K}, \quad P_{SI} = \frac{N_{SI}}{K} \quad \text{and} \quad P_{II} = \frac{N_{II}}{K}. \tag{1.8a}$$

By using the moment closure approximations (1.6) and conservation of nodes $P_S + P_I = 1$ and links $P_{II} + P_{SS} + P_{SI} = 1$, we obtain a closed 3 dimensional system of equations:

$$\frac{dP_I}{dt} = -rP_I + \frac{p\kappa}{2}P_{SI}, \tag{1.9a}$$

$$\frac{dP_{SS}}{dt} = (r+w)P_{SI} - p\kappa\frac{P_{SI}P_{SS}}{(1-P_I)}, \tag{1.9b}$$

$$\frac{dP_{SI}}{dt} = 2r(1-P_{SS}-P_{SI}) - (p+r+w)P_{SI} + p\kappa\frac{P_{SS}P_{SI}}{(1-P_I)} - \frac{p\kappa}{2}\frac{P_{SI}^2}{(1-P_I)}, \tag{1.9c}$$

where $\kappa = \frac{2K}{N}$. If we solve Eqs. (1.9) at the steady state, a unique disease-free state (DFS) for $P_I = 0$ is obtained. For $P_I \neq 0$, a quadratic equation is obtained, whose solutions are the two nontrivial states of the system. The stability of these states were studied numerically in [7]. However, we study analytically the stability of these states in the following sections.

1.3.1 Local stability analysis of the disease-free state

For $p > 0$, $(P_{\mathrm{I}}, P_{\mathrm{SS}}, P_{\mathrm{SI}}) = (0, 1, 0)$ is the unique disease-free state (DFS) of Eqs. (1.9). The Jacobian matrix evaluated at the DFS is

$$\mathbf{J} = \begin{pmatrix} -r & 0 & p\kappa/2 \\ 0 & 0 & r + w - p\kappa \\ 0 & -2r & -3r - w + p\kappa - p \end{pmatrix}. \tag{1.10}$$

To find the eigenvalues λ of the Jacobian matrix, we solve

$$\det(\mathbf{J} - \lambda \mathbf{I}) = 0 \tag{1.11a}$$

$$(\lambda + r)\left[\lambda^2 + \lambda(2r + p + B) + 2rB\right] = 0 \tag{1.11b}$$

for λ, where $B = r + w - p\kappa$. One of the eigenvalues is $\lambda_1 = -r$, and if $B > 0$ then $Re(\lambda_2) < 0$ and $Re(\lambda_3) < 0$. However, if $B < 0$ then one of the eigenvalues will have a positive real part. Therefore, the DFS is locally stable if $p < (r + w)/\kappa$ and unstable otherwise. This critical value of infection rate

$$p^* = \frac{(r + w)}{\kappa} \tag{1.12}$$

is called by the *epidemic threshold.* Small perturbations away from the DFS will grow for $p > p^*$, i.e., an epidemic will spread through the population if the infection rate is greater than the epidemic threshold.

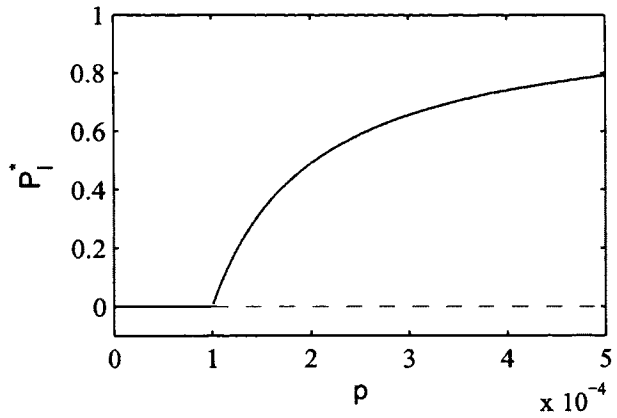

Figure 1.1: Bifurcation diagram for the fraction of infecteds in a static network ($w = 0$) as a function of infection rate p for $r = 0.002$ and $\kappa = 20$. Solid black curve: stable solution, dashed gray curve: unstable solution.

1.3.2 Local stability analysis of the endemic state

For $P_{SI} \neq 0$, solving Eqs. (1.9) at the steady state yields the link variables as a function of P_I:

$$P_{SI} = \frac{2r}{p\kappa} P_I \tag{1.13a}$$

$$P_{SS} = \frac{r+w}{p\kappa}(1 - P_I) \tag{1.13b}$$

Substituting Eqs. (1.13) into Eq. (1.9c), and using conservation of links, we obtain

$$\frac{2r}{p\kappa} P_I + \frac{r+w}{p\kappa}(1 - P_I) + \frac{r}{p\kappa}\frac{P_I^2}{1 - P_I} + \frac{1}{\kappa} P_I = 1 \tag{1.14}$$

Multiplying by $(1 - P_I)p\kappa$,

$$(w - p)P_I^2 + (p - 2w + p\kappa)P_I + (r + w) - p\kappa = 0 \tag{1.15}$$

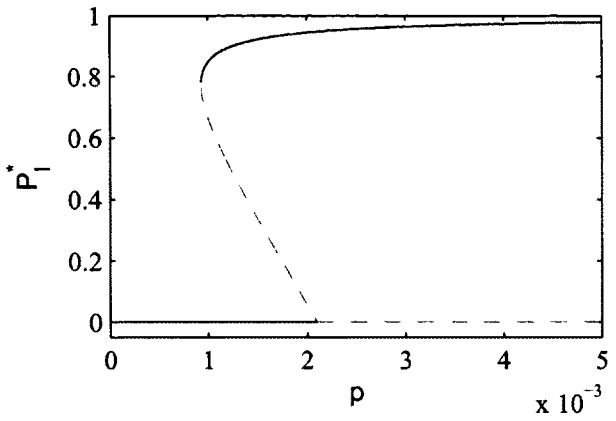

Figure 1.2: Bifurcation diagram for the fraction of infecteds in an adaptive network as a function of infection rate p for $w = 0.004$, $r = 0.002$ and $\kappa = 20$. Solid black curve: stable solution, dashed gray curve: unstable solution.

Static case:

Letting $P_I = x$, then for a static network ($w = 0$),

$$x^2 - (1 + \kappa)x + \kappa - r/p = 0 \tag{1.16}$$

There are two solutions of Eq. (1.16)

$$x_1 = \frac{(\kappa + 1) + \sqrt{(\kappa - 1)^2 + 4r/p}}{2} \tag{1.17a}$$

$$x_2 = \frac{(\kappa + 1) - \sqrt{(\kappa - 1)^2 + 4r/p}}{2} \tag{1.17b}$$

$x_1 > 1$ for all κ ($p > 0$, $r > 0$). Since we defined $x = P_I$ as a probability, x_1 can not be a realistic solution of the endemic state. If $p < r/\kappa$ then $x_2 < 0$; otherwise $0 < x_2 < 1$ which is the endemic solution. A new branch of steady state solution emerges at $p = r/\kappa$, which is the epidemic threshold we found in Eq. (1.12). Thus, at this bifurcation point, the disease-free branch and the endemic branch intersect and the DFS loses stability for $p > p^*$. We conclude that this is a forward transcritical bifurcation since there is no other realistic solution of Eq. (1.16) at $p = r/\kappa$ (see Fig. 1.1).

Adaptive case:

For the adaptive network case the endemic states are the solutions of the quadratic equation

$$(p-w)x^2 + (2w-p-p\kappa)x + p\kappa - w - r = 0 \tag{1.18}$$

Substituting these solutions into Eqs. (1.13), and finding the eigenvalues of the Jacobian at these points, we can numerically study the stability of the two endemic branches. As we see in Fig. 1.2, the upper branch loses stability at a saddle-node bifurcation point for $w = 0.04$. For larger values of w ($w = 0.2$), a Hopf bifurcation was observed in [7].

At the epidemic threshold $p^* = (w + r)/\kappa$, there are two solutions:

$$x_1 = 0 \quad \text{and} \quad x_2 = \frac{p + p\kappa - 2w}{p - w} \tag{1.19}$$

For the appropriate choice of parameters p, w and κ, we can guarantee that $x_2 \in (0, 1)$. Therefore, there is a nonzero solution at the epidemic threshold, which shows that the system undergoes a backward transcritical bifurcation point at the threshold. Therefore, a region of bistability exists, where both the DFS and endemic state are stable. The spread of disease in this region will depend on the initial conditions. For the values of p in this region, small perturbations from the DFS will not grow, in contrast to non-adaptive case.

Chapter 2

Effects of community structure on epidemic spread in an adaptive network

2.1 Summary

When an epidemic spreads in a population, individuals may adaptively change the structure of their social contact network to reduce risk of infection. In this chapter, we study the spread of an epidemic on an adaptive network with community structure. We model two communities with different average degrees. The disease model is susceptible-infected-susceptible (SIS), and adaptation is rewiring of links between susceptibles and infectives. Locations of rewired links are selected so that the community structure will be preserved if susceptible-infective links are homogeneously distributed. The bifurcation structure is obtained, and a mean field model is developed that accurately predicts the steady state behavior of the system. In a static network, weakly connected heterogeneous communities can have significantly different infection levels. In contrast, adaptation promotes similar infection levels and alters the network structure so that communities have more similar average degrees. We estimate the time for network restructuring to allow infection incursion

from one community to another and show that it is inversely proportional to the number of cross links between communities. In extremely heterogeneous systems, periodic oscillations in infection level can occur due to repeated infection incursions.

The results of this chapter have been submitted to *Physical Review E* as "Effects of community structure on epidemic spread in an adaptive network" by Ilker Tunc and Leah B. Shaw.

2.2 Introduction

In recent years, networks have been widely used in modeling a variety of social, technological, and biological systems [5, 3, 4]. One major application is modeling the spread of an epidemic on a social network (e.g., [26, 27, 28, 29, 30]). In these models, typically the network structure is assumed static, while the infection status of the nodes changes dynamically.

During an epidemic, people may tend to avoid social connections with infected individuals [7, 9]. This system can be considered an adaptive network, where the node dynamics affects the network topology, which then affects future changes in node status [8]. Epidemic spreading in adaptive network models with avoidance behavior has been studied previously [7, 14, 8, 11, 12, 13], with avoidance frequently implemented via susceptible nodes rewiring their links away from infected neighbors and towards other non-infected nodes. Changes in bifurcation structure have been observed, including the existence of bistable regimes with endemic and disease-free states both stable.

One of the most important features of a social network is community structure [16]. The strength of the community structure can be quantified by using a modularity measure [16], which for a random network will be close to zero, and will be close to one for a strong community structure.

Studies of epidemics with community structure have focused mainly on static network geometries, including scale-free [31, 32, 33], small-world [34] and random networks [35]. It has been found that community structure can either decrease [32] or increase [35] infection prevalence, depending on details of the model. Further, epidemics can synchronize

across communities if there are sufficient connections between communities [31, 34]. In a dynamic but not adaptive example, communities of mobile agents were studied [36, 37], and dynamic hopping of agents between communities was able to produce sustained infection in communities that were below the epidemic threshold if other communities were above threshold.

Adaptive networks with community structure have been studied only rarely. In [38], the authors considered an adaptive scale-free network with community structure in which neighbors of an infected node can move to other communities with a certain probability. Infection levels were reduced compared to the case without adaptation, but the adaptation mechanism did not preserve the community structure as measured by modularity. In [39], the authors introduced a model very similar in structure to the one we will consider here. However, their focus was to study an adaptive epidemic system with two types of agents. They varied the within-type and cross-type link rewiring rates and infection rates and determined their effects on the size of the bistability region. For certain parameter choices the endemic steady state would have a community structure, but the resulting structure was not characterized in this study.

In this chapter, we extend the adaptive susceptible-infected-susceptible (SIS) model of [7] to a network with two communities. In contrast to previous studies [38, 39], we allow the communities to have different average degrees. We define rewiring rules such that the community structure is preserved if links between susceptibles and infectives are uniformly distributed. We directly simulate the stochastic network system and derive a lower dimensional mean field, based on a moment closure approximation, that accurately predicts the bifurcation structure of the full system. In Section 2.3, we define the model and introduce the mean field equations. Results in the absence of adaptation are presented in Subsection 2.4.1. In Subsection 2.4.2, we show the effects of adaptation on the bifurcation structure and on the network geometry. Section 2.5 concludes.

2.3 Model

We study a susceptible-infective-susceptible (SIS) model on an adaptive network having two communities. The communities are labeled A and B and consist of N_a and N_b nodes, respectively. In this chapter $N_a = N_b = 5000$. We use two probability parameters to generate an initial network with two communities by creating links. Parameter $d \in [0,1]$ determines the asymmetry in average degree of the communities, and $f \in [0,1]$ determines the number of links between communities. Links are created as follows. With probability d we choose a node among the N_a nodes in community A (otherwise choosing a node in community B), and with probability f its neighbor is chosen at random from the opposite community as the first node (otherwise choosing from the same community). Self links and multiple links are disallowed. This process is repeated until a total of K links are created. We use $K = 10^5$ throughout this chapter. At this point a fraction $(1-f)d$ of the links are AA, $(1-f)(1-d)$ are BB, and f are AB. The average degrees in communities A and B are

$$\langle k_a \rangle = \frac{K}{N_a}\left[2(1-f)d + f\right] \qquad \text{and} \qquad \langle k_b \rangle = \frac{K}{N_b}\left[2(1-f)(1-d) + f\right],$$

respectively. Thus the communities are symmetric when $d = 0.5$. We will focus here on the case $d > 0.5$, so community A will have higher connectivity than B. The total number of cross links between communities is fK.

We define node dynamics as in [7]. A susceptible (S) node becomes infected with rate pN_{inf}, where N_{inf} is the number of infected neighbors the node has and p is the infection rate. An infected (I) node recovers with recovery rate r. One of these rates can be eliminated by rescaling time, so it is sufficient to treat r as fixed. We fix $r = 0.002$ throughout the chapter as in previous studies [7, 11] .

Network adaptation in the form of avoidance behavior is introduced by allowing susceptible infected links to rewire with rate w to susceptible-susceptible links, as in [7]. However, the rewiring must be adjusted to retain the desired community structure. This is done by choosing the susceptible node's new neighbor from one or the other community with

appropriate probabilities. An S node having an infected neighbor rewires to an S node in the same community as itself with probability α if the S node is in community A and with probability β if the S node is in community B. Otherwise a neighbor in the other community is selected. In order to retain the community structure, we set

$$\alpha = \frac{2(1-f)d}{2(1-f)d+f} \qquad \text{and} \qquad \beta = \frac{2(1-f)(1-d)}{2(1-f)(1-d)+f}$$

This choice is made so that if randomly selected links rewire, then the flux from AA links to AB links, $(1-f)d(1-\alpha)$, equals the flux from AB links to AA links, $f/2\alpha$, and likewise for balance of fluxes between BB and AB links. Therefore, if SI links occur at random anywhere in the network, this rewiring strategy will on average keep the community structure specified above by d and f.

We simulate our model using Gillespie's method [40] for $N = 10^4$ nodes and $K = 10^5$ links [11]. The initial condition is either the final state of a previous run or a random two-community network constructed as described above in which a fraction of the nodes have been randomly infected. As in [7, 11], we derive mean field equations for the evolution of the nodes and links. P_X denotes the probability of nodes to be in state X, where X is susceptible in community A or B (S_a or S_b) or infected in A or B (I_a or I_b). P_{XY} denotes the probability that a randomly selected link connects a node in state X to a node in state Y. We obtain the following equations for the node dynamics:

$$\dot{P}_{I_a} = -rP_{I_a} + \frac{pK}{N_a}(P_{S_aI_a} + P_{S_aI_b}) \tag{2.1}$$

$$\dot{P}_{I_b} = -rP_{I_b} + \frac{pK}{N_b}(P_{S_bI_a} + P_{S_bI_b}) \tag{2.2}$$

Because nodes are neither created nor destroyed and do not change their community assignment, the equations for susceptibles in community A and B can be found from node conservation. The evolution of the links depends on three point terms. As in [7, 14, 11] we use a moment closure assumption to close the system, assuming $P_{XYZ} \approx P_{XY}P_{YZ}/P_Y$, where P_{XYZ} is the fraction of three point terms. After applying the moment closure, the

link equations are

$$\dot{P}_{S_aS_a} = rP_{S_aI_a} + w\alpha(P_{S_aI_a} + P_{S_aI_b}) - \frac{2pK}{N_a}(\frac{P_{S_aS_a}P_{S_aI_a}}{P_{S_a}} + \frac{P_{S_aS_a}P_{S_aI_b}}{P_{S_a}}) \tag{2.3}$$

$$\dot{P}_{S_bS_b} = rP_{S_bI_b} + w\beta(P_{S_bI_a} + P_{S_bI_b}) - \frac{2pK}{N_b}(\frac{P_{S_bS_b}P_{S_bI_a}}{P_{S_b}} + \frac{P_{S_bS_b}P_{S_bI_b}}{P_{S_b}}) \tag{2.4}$$

$$\begin{aligned}\dot{P}_{S_aS_b} &= rP_{S_bI_a} + rP_{S_aI_b} + w(1-\alpha)(P_{S_aI_a} + P_{S_aI_b}) + w(1-\beta)(P_{S_bI_a} + P_{S_bI_b}) \\ &\quad - \frac{pK}{N_a}(\frac{P_{S_bS_a}P_{S_aI_a}}{P_{S_a}} + \frac{P_{S_bS_a}P_{S_aI_b}}{P_{S_a}}) - \frac{pK}{N_b}(\frac{P_{S_aS_b}P_{S_bI_a}}{P_{S_b}} + \frac{P_{S_aS_b}P_{S_bI_b}}{P_{S_b}})\end{aligned} \tag{2.5}$$

$$\begin{aligned}\dot{P}_{S_aI_a} &= 2rP_{I_aI_a} - (r+p+w)P_{S_aI_a} \\ &\quad + \frac{2pK}{N_a}(\frac{P_{S_aS_a}P_{S_aI_a}}{P_{S_a}} + \frac{P_{S_aS_a}P_{S_aI_b}}{P_{S_a}}) - \frac{pK}{N_a}(\frac{P^2_{S_aI_a}}{P_{S_a}} + \frac{P_{S_aI_a}P_{S_aI_b}}{P_{S_a}})\end{aligned} \tag{2.6}$$

$$\begin{aligned}\dot{P}_{S_bI_b} &= 2rP_{I_bI_b} - (r+p+w)P_{S_bI_b} \\ &\quad + \frac{2pK}{N_b}(\frac{P_{S_bS_b}P_{S_bI_a}}{P_{S_b}} + \frac{P_{S_bS_b}P_{S_bI_b}}{P_{S_b}}) - \frac{pK}{N_b}(\frac{P^2_{S_bI_b}}{P_{S_b}} + \frac{P_{S_bI_b}P_{S_bI_a}}{P_{S_b}})\end{aligned} \tag{2.7}$$

$$\begin{aligned}\dot{P}_{S_aI_b} &= rP_{I_aI_b} - (r+p+w)P_{S_aI_b} \\ &\quad + \frac{pK}{N_b}(\frac{P_{S_aS_b}P_{S_bI_a}}{P_{S_b}} + \frac{P_{S_aS_b}P_{S_bI_b}}{P_{S_b}}) - \frac{pK}{N_a}(\frac{P^2_{S_aI_b}}{P_{S_a}} + \frac{P_{S_aI_b}P_{S_aI_a}}{P_{S_a}})\end{aligned} \tag{2.8}$$

$$\begin{aligned}\dot{P}_{S_bI_a} &= rP_{I_aI_b} - (r+p+w)P_{S_bI_a} \\ &\quad + \frac{pK}{N_a}(\frac{P_{S_bS_a}P_{S_aI_a}}{P_{S_a}} + \frac{P_{S_bS_a}P_{S_aI_b}}{P_{S_a}}) - \frac{pK}{N_b}(\frac{P^2_{S_bI_a}}{P_{S_b}} + \frac{P_{S_bI_a}P_{S_bI_b}}{P_{S_b}})\end{aligned} \tag{2.9}$$

$$\dot{P}_{I_aI_a} = -2rP_{I_aI_a} + pP_{S_aI_a} + \frac{pK}{N_a}(\frac{P^2_{S_aI_a}}{P_{S_a}} + \frac{P_{S_aI_a}P_{S_aI_b}}{P_{S_a}}) \tag{2.10}$$

$$\dot{P}_{I_bI_b} = -2rP_{I_bI_b} + pP_{S_bI_b} + \frac{pK}{N_b}(\frac{P^2_{S_bI_b}}{P_{S_b}} + \frac{P_{S_bI_b}P_{S_bI_a}}{P_{S_b}}) \tag{2.11}$$

$$\begin{aligned}\dot{P}_{I_aI_b} &= -2rP_{I_aI_b} + p(P_{S_aI_b} + P_{S_bI_a}) \\ &\quad + \frac{pK}{N_a}(\frac{P^2_{S_aI_b}}{P_{S_a}} + \frac{P_{S_aI_b}P_{S_aI_a}}{P_{S_a}}) + \frac{pK}{N_b}(\frac{P^2_{S_bI_a}}{P_{S_b}} + \frac{P_{S_bI_a}P_{S_bI_b}}{P_{S_b}})\end{aligned} \tag{2.12}$$

These mean field equations are a special case of the general mean field in [39] for appropriate choices of their rewiring and infection parameters.

Since the total number of links is fixed, we have an 11 dimensional system in the adaptive network case by eliminating one of the link equations. On the other hand, we have a 9 dimensional system in the static network case because the numbers of AA, AB, and BB links are each fixed. These equations can be integrated with standard numerical integration methods. Also, we tracked their steady states using a continuation package [41].

2.4 Results

2.4.1 Static network

We first consider the effect of having two communities with different average connectivities in a static network ($w = 0$). We obtained the bifurcation structure (Fig. 2.1) as follows. We used the XPPAUT free software package [41] to locate the stable and unstable equilibrium solutions of the mean field equations. To obtain the steady states of the full system, we generated an initial random network with community structure in which 50% of the nodes were infected. To locate the upper branch (endemic state), the system was run to steady state for a high infection rate p, and p was decreased gradually using the final state of each run as an initial state for the next run. For each p, we ran the system up to 5×10^4 time units and then averaged the steady state over 500 samples where there are 10^3 events between each sample. To locate the lower branch (disease-free state), we generated five different realizations of a random network with community structure in which 2.5% of the nodes were infected. The system was simulated for 5×10^4 time units, and the results were obtained for the five network realizations for each p value. If the infected fraction went to zero in any of the five runs, the disease-free state was considered stable. As shown in Fig. 2.1, the mean field equations and the full system are in good agreement.

In a static network without community structure, the disease-free state loses stability at a critical infection rate p^* where the system undergoes a transcritical bifurcation. This threshold infection rate depends on the average degree of the network [7]. Figure 2.1(a) superimposes the bifurcation diagrams of two single-community networks with different

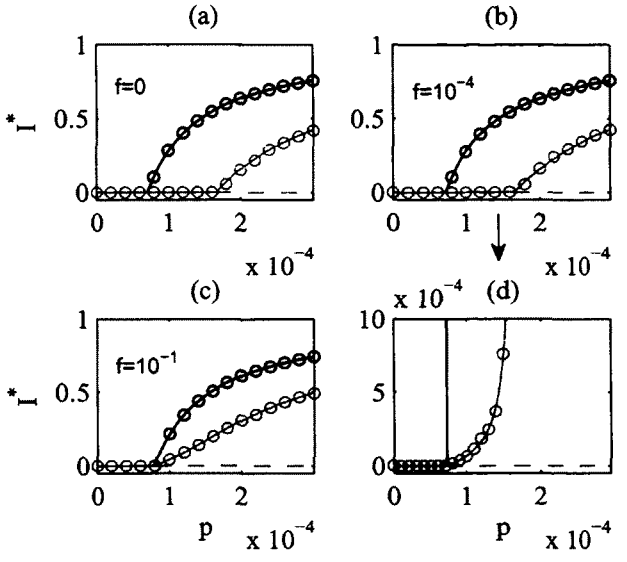

Figure 2.1: Bifurcation diagram for infected fraction in a static network ($w = 0$) as a function of infection rate p for different fractions of cross links f. Black: community A; gray: community B. Solid curves: mean field solutions (stable branches); dashed curves: mean field solutions (unstable branches); circles: Monte Carlo simulations. Average degrees $\langle k_a \rangle \approx 28$ and $\langle k_b \rangle \approx 12$. The plots correspond to $d = 0.7$. In (d), in order to obtain better statistics, we averaged over 100 network realizations, each of which is similar to (b).

average degrees. The epidemic threshold for community A (p_a^*) and community B (p_b^*) are significantly different. When the two networks are loosely connected ($f = 10^{-4}$, Fig. 2.1(b) and blowup in Fig. 2.1(d)), the combined system has a single threshold infection rate, which is approximately p_a^* and much lower than p_b^* in the disconnected case. When the infection rate is between p_a^* and p_b^*, the fraction of infecteds in B is close to zero (Fig. 2.1(d)) and stochastic reintroduction of infection from A to B is observed. However, when the two communities are strongly connected ($f = 10^{-1}$, Fig. 2.1(c)), they behave similarly in that both communities have significant infection levels for the same parameter values.

Although a system of two connected communities has an infection threshold at a single bifurcation point, we wish to distinguish between the cases in Fig. 2.1(b), 2.1(c), where significant infection spread occurs in the low degree community (B) if it has sufficient links to the high degree community (A), while the infection in community B is very small if the number of cross links is low. To quantify this, we define effective threshold infection rates

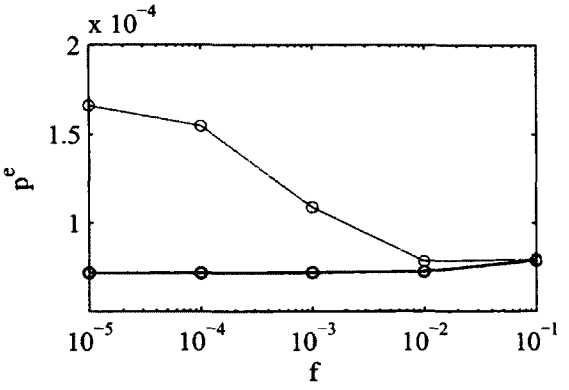

Figure 2.2: Effective threshold infection rate from mean field vs fraction of cross links f for $d = 0.7$. Black curve: community A; gray curve: community B. The infection rate p at which the fraction of infecteds is less than 10^{-3} is considered the effective threshold rate.

p_a^e, p_b^e for each community as follows. While sweeping the infection rate p from higher to lower values, the first p value at which the fraction of infecteds at the steady state is lower than $\epsilon = 10^{-3}$ is considered as the effective threshold infection rate for that community. Figure 2.2 shows the effective threshold infection rates versus cross link fraction f. When $f < 10^{-2}$, the effective thresholds in the two communities become noticeably different.

2.4.2 Adaptive network

We now move to systems with nonzero rewiring rates. The bifurcation structure for the adaptive network case was determined as for static networks except for the following modification. In our model, network adaptation does not occur in the absence of infection. This means that the DFS of Eqs. (2.1)-(2.12) is not isolated, because any disease-free combination of AA, AB, and BB links is a steady state. Because of the non-isolated fixed points, the stability of the disease-free branch could not be determined using continuation packages. Instead, we calculated numerically the eigenvalues of the Jacobian evaluated at the DFS for the initial network geometry which is described by f and d.

In the absence of community structure ($f = 0$), the DFS loses stability at a critical infection rate p^*, where the unstable endemic branch and the stable disease-free branch intersect at a transcritical bifurcation (Fig. 2.3(a)). The epidemic threshold p^* is inversely

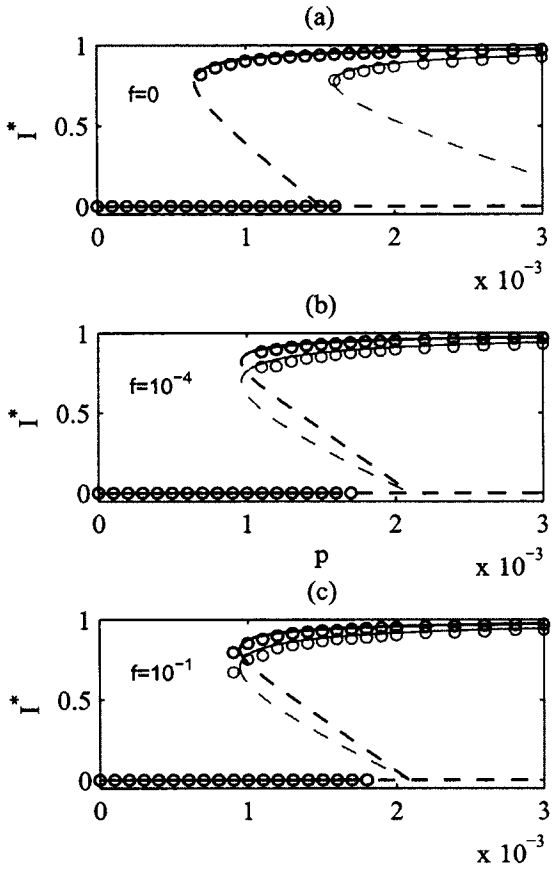

Figure 2.3: Bifurcation diagram for infected fraction in an adaptive network as a function of infection rate p for different fractions of cross links f. Black: community A; gray: community B. Solid curves: mean field solutions (stable branches); dashed curves: mean field solutions (unstable branches); circles: Monte Carlo simulations. Average degrees $\langle k_a \rangle \approx 28$ and $\langle k_b \rangle \approx 12$. The plots correspond to $d = 0.7$ and $w = 0.04$. The simulations are done similarly as in Fig. 2.1, but here we run the system for 5×10^6 time units in order to approach the endemic branch.

proportional to the average degree of the network and can be found analytically from the Jacobian of the mean field equations for a single network (Eq. 1.12).

For a network having two loosely connected heterogeneous communities ($f = 10^{-4}, d = 0.7$), p^* is very close to that of a single network having the same average degree as community A (Fig. 2.3(a), 2.3(b)). This is expected because when the infection in community A starts to spread, a small value of f will not be enough to stop infection spreading in community A. In contrast, for $f = 10^{-1}$, p^* is larger than that of a single network having the same average degree as community A. In this case, the connection is stronger and the infection starting to spread in community A can be suppressed by the connection to a community where no infection is observed. As we increase f, the critical value of p approaches that of a single network with average degree $\langle k \rangle = 20$, which is the average degree in the entire system.

In an adaptive network without community structure, bistability can occur for a range of rewiring rates [7]. We focus on the rewiring rate $w = 0.04$, for which the endemic branch loses stability at a critical infection rate where the system undergoes a saddle-node (SN) bifurcation. The location of this SN bifurcation depends on the average degree of the network. Figure 2.3(a) superimposes the bifurcation diagrams of two single-community networks with different average degrees. In our model, for a network having two strongly connected communities ($f = 10^{-1}$), the endemic state loses stability at a SN bifurcation point. However, for the loosely connected case ($f = 10^{-4}$), the endemic branch loses stability at a Hopf bifurcation (HB) point. As with the epidemic threshold (transcritical bifurcation) in static networks, the location of the SN bifurcation and the HB in the adaptive network is governed primarily by the high degree community. However, in contrast with the static case, small cross link fraction f is not associated with low steady state infection levels in the low degree community. As will be seen later in this section, the state with high infection in one community and low in the other community is not a steady state due to the network adaptation. Instead, infection levels are similar in both communities even if weakly connected. Both communities continue to exhibit high infection levels as the number

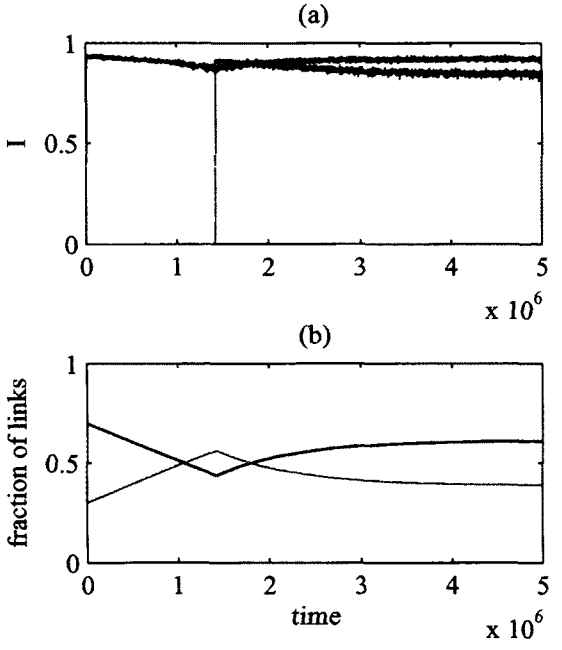

Figure 2.4: Time series from Monte Carlo simulation of full system. (a) Infected node fractions. Black curve: fraction of infecteds in community A; gray curve: fraction of infecteds in community B. (b) Fraction of links. Black curve: fraction of AA type links; gray curve: fraction of BB type links. Initial condition is as described in the text. $f = 10^{-4}$, $d = 0.7$, $w = 0.04$ and $p = 0.0014$.

of cross links is further increased (Fig. 2.3(c)). By looking at the time series of the mean field equations, we observed a stable periodic solution for a very small range of p values near the HB point. However, we do not see any periodic behavior in the full system due to the narrow range of p values. As the heterogeneity in the network increases by increasing d, the Hopf bifurcation point also increases. Furthermore, the epidemic threshold increases because of a much higher average degree in community A. This narrows the region where both disease-free and endemic branches are stable. In particular, for $d = 0.9$, there is no p value where both the endemic steady state and DFS are stable. For $d = 0.9$ we observed periodic solutions with a very long period for p values smaller than the HB point in both mean field and the full system.

To motivate the absence of the state seen in static networks with high infection in one community and low infection in the other, we consider a long time series starting initially with a randomly generated two-community network, generated as described in Section 2.3,

where $f = 10^{-4}$, $d = 0.7$, and we infect a random 50% of the nodes. As seen in Fig. 2.4, the fractions of AA and BB type links change with time. The adaptation rules have been chosen so that if SI links are distributed uniformly throughout the network, the community structure will be preserved. In a fast transient which can not be seen in the time scale of Fig. 2.4, the fraction of infecteds in both of the communities approaches the limit expected for single networks, high in community A and extinction in community B. However, with high initial infection levels in A and low in B, there are more SI links among the AA and AB links and fewer among the BB links. This leads to a net flux of link types from AA to AB to BB. (The fraction of AB links (not shown) remains relatively constant at low levels throughout.) Eventually the average degree in the B community exceeds that in the A community and there is an incursion of infection from A to B. The flux of link types is then reversed, and the steady state network structure is similar (but not identical) to that expected from the community structure parameters d, f. The infection persists at high levels in both communities at steady state.

We can estimate the time until infection incursion in the B community as follows. From Eqs. (2.3), (2.6), (2.10), the fraction of AA links $P_{aa} = P_{S_aS_a} + P_{S_aI_a} + P_{I_aI_a}$ evolves according to

$$\dot{P}_{aa} = w\left[\alpha P_{S_aI_b} - (1-\alpha)P_{S_aI_a}\right]. \tag{2.13}$$

Since we are interested in the critical time when infection starts to spread in community B, we can assume $P_{I_b} \approx 0$ and hence $P_{S_aI_b} \approx 0$. Thus

$$\begin{aligned}\dot{P}_{aa} &\approx -w(1-\alpha)P_{S_aI_a} \\ &\approx -w(1-\alpha)\gamma P_{aa},\end{aligned} \tag{2.14}$$

where $\gamma = P_{S_aI_a}/P_{aa}$. Since f is close to zero, we can use the single community mean field equations to approximate γ, the fraction of SI links in community A (Eqs. 1.13), which we will assume here to stay approximately constant.

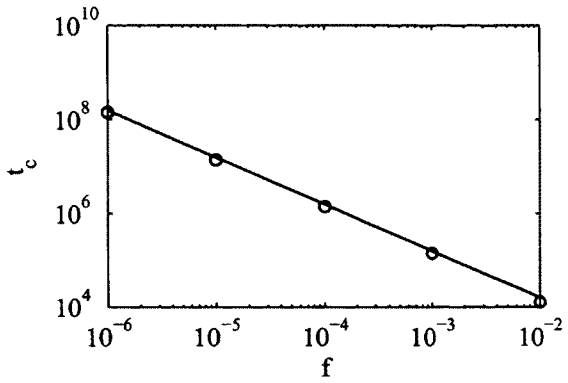

Figure 2.5: The critical time for infection incursion in community B vs fraction of cross links f. The critical time values are averaged over 5 runs except for $f = 10^{-6}$. In each run, the time when the fraction of infecteds in community B exceeded 0.1% is considered the critical time. Initial condition for each run is a two-community network randomly generated as in Fig. 2.4. The symbols show the simulation results, the solid line has slope -1.

We can then solve Eq. (2.14) for the critical time t_c for infection incursion if we know P_{aa} at that time. Since we can predict the critical average degree for community B (Eq. 1.12) in order for the disease to spread, we can also find P_{aa} at that point. So, we can solve the equation for t_c as follows:

$$t_c \approx \ln\left[\frac{P_{aa}(0)}{P_{aa}(t)}\right][w(1-\alpha)\gamma]^{-1} \tag{2.15}$$

from which it can be shown that the critical time t_c is proportional to $1/(1-\alpha)$. For f close to zero, $1-\alpha \approx f/2d$, therefore $t_c \propto 1/f$. In Fig. 2.5, we can see that this relationship holds for the full system. However, we note that for the full system, the infection in community B starts to spread approximately 50% earlier than the time found by using mean field equations for $d = 0.7$.

When the system reaches steady state (late time in Fig. 2.4), the network geometry does not return exactly to that expected from the community structure parameters f, d because the SI links are not uniformly distributed. This effect is most pronounced when the infection rate is below the critical infection rate for the low connectivity network, because then the SI link distribution is the most nonuniform. Figure 2.6 shows the steady state community structure versus the infection rate. Deviations from the community structure

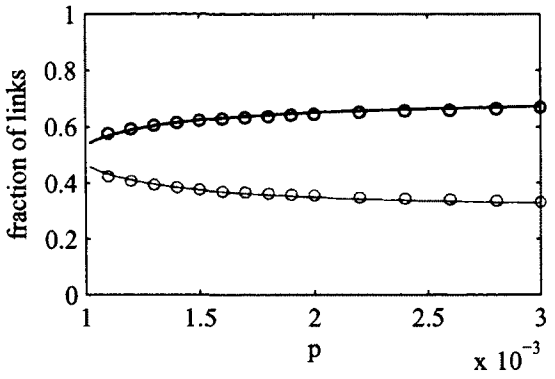

Figure 2.6: Fraction of links vs infection rate p. Curves: mean field steady states; points: Monte Carlo steady state averages. Black: fraction of AA type links; gray: fraction of BB type links. (The fraction of AB links is less than 1%.) $f = 10^{-4}$, $d = 0.7$ and $w = 0.04$. The data is from the simulations done in Fig. 2.3.

specified by f, d increase as the infection rate approaches the Hopf bifurcation point at $p \approx 0.0019$. Thus the steady state average degree observed in the two communities in the presence of an epidemic can be different than that expected in the absence of an epidemic. The adaptation has a homogenizing effect, bringing the degrees in the communities closer to each other.

For $d = 0.9$, different dynamics are observed following infection incursion in the low degree community. In Fig. 2.7, we started with similar initial conditions as for $d = 0.7$ in Fig. 2.4. The system behaved similarly for a long time, but once the infection level reached a high value in community B, it could not stay in that state, because a higher d means a higher flux out from BB type links. The average degree in B started to decrease, causing infection to die out again in community B. A periodic solution with a long period is observed for a range of p values.

2.5 Conclusions

We have studied epidemic spread in a network of two communities with different average degrees. Cases with and without disease avoidance rewiring were considered. Rewiring rules were chosen so that the community structure would be preserved if links between

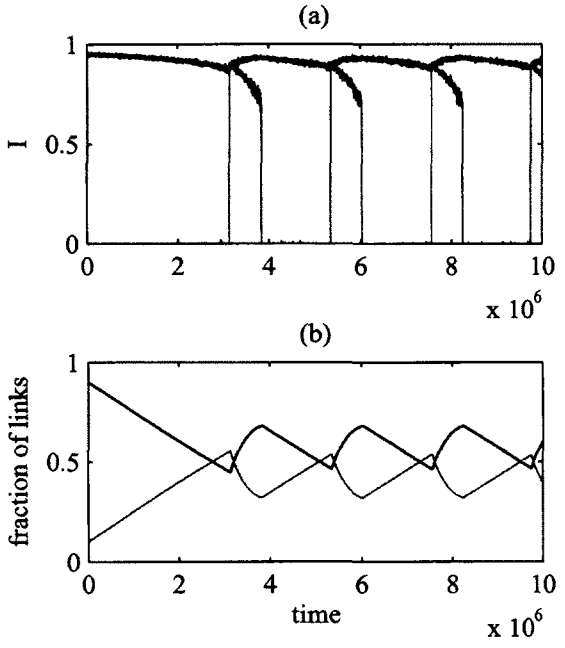

Figure 2.7: Time series from Monte Carlo simulation of full system. (a) Infected node fractions. Black curve: fraction of infecteds in community A; gray curve: fraction of infecteds in community B. (b) Fraction of links. Black curve: fraction of AA type links; gray curve: fraction of BB type links. Initial condition is as described in the text. $d = 0.9$, $w = 0.04$ and $p = 0.0014$.

susceptibles and infectives occurred uniformly throughout the network. The steady state bifurcation structure was obtained for static and adaptive cases. A mean field theory based on a moment closure approximation accurately predicted the steady state infection levels and network structure observed in stochastic simulations of the full model.

In the static network case, weakly connected communities displayed significantly different infection levels. Low infection levels could persist in a subthreshold community weakly connected to a high degree, high infection community. Increasing the number of connections between communities led to more similar behavior of the two communities. In contrast, communities in adaptive networks displayed similar infection levels even if weakly connected. Steady states with high infection in one community and low in the other did not exist for the adaptive network case.

The absence of steady states with significantly different infection levels was explained by considering network adaptation in the presence of nonuniformly distributed SI links. If one community has few infectives, there is a net flux of links into that community until its degree is high enough to support the infection. We estimated the time until this infection incursion based on mean field arguments and found that the time increases as the number of cross links between communities decreases.

We also observed changes in the steady state network geometry due to adaptation in the presence of infection. These changes were most significant near bifurcation points. The adaptation tended to bring the average degrees of the communities closer to each other. Thus the adaptation promotes greater similarity between communities in both network structure and infection levels.

The model presented in this chapter is the first to include community structure in epidemic spread on an adaptive network. Future work is needed to extend the model to more realistic scenarios. For example, the number of communities could be increased beyond two. We have observed that the convergence time to steady state can be very long for weakly coupled communities, so it is possible that an epidemic would not reach steady state during physically realistic time scales. Thus the transient behavior should also be studied in more

detail. Identifying when communities become at risk for incursion of infection could be valuable in knowing when epidemic control measures are needed. Another area for future extension is to change the rules for adaptation, such as cutting or temporarily deactivating links rather than rewiring them [42].

Chapter 3

Epidemics in adaptive social networks with temporary link deactivation

3.1 Summary

Disease spread in a society depends on the topology of the network of social contacts. Moreover, individuals may respond to the epidemic by adapting their contacts to reduce the risk of infection, thus changing the network structure and affecting future disease spread. In this chapter, we propose an adaptation mechanism where healthy individuals may choose to temporarily deactivate their contacts with sick individuals, allowing reactivation once both individuals are healthy. We develop a mean field description of this system and find two distinct regimes: slow network dynamics, where the adaptation mechanism simply reduces the effective number of contacts per individual, and fast network dynamics, where more efficient adaptation reduces the spread of disease by targeting dangerous connections. Analysis of the bifurcation structure is supported by numerical simulations of disease spread on an adaptive network. The system displays a single parameter-dependent stable steady state and non-monotonic dependence of connectivity on link deactivation rate.

The results of this chapter have been published in the Journal of Statistical Physics [42].

3.2 Introduction

In classical compartmental epidemic models, it is assumed that the population is homogeneously mixed, and every individual has an equal chance to contact any other individual in the population [1]. As this assumption is relaxed, the social network topology is included [4, 5, 6]. Furthermore, disease spread on both static [28, 29, 26, 30] and evolving [43, 44] networks are considered.

A class of epidemic models that recently has received a lot of attention considers the situation where people may change their social preferences during an epidemic to avoid exposure to disease [8, 9]. These models try to take into account the effect that the presence of the disease can have on the network topology. The individuals in the society may choose to adapt their local connections based on the desire to quarantine themselves from the epidemic. This in turn affects the further spread of the disease. Some models consider rewiring of potentially dangerous connections as the adaptation mechanism [7, 14, 11, 15]. That is, when a contact between individuals is abandoned, a new contact is immediately formed, and the total number of connections is conserved. A motivation for these models is that social connections serve a purpose, and thus a fixed number of connections must be maintained for society to continue functioning. In the first models of this type, a healthy individual breaks its connection with a sick individual, in favor of some other healthy individual [7, 11]. The assumption in this model is that each person knows the infection status of all the people in the society. In [14], relaxing this assumption, a healthy person reconnects to a randomly chosen person. Furthermore, sick individuals may altruistically rewire their links away from their healthy contacts [15]. With rewiring as the adaptation mechanism, bistability is frequently observed, where both the disease-free state and endemic state coexist for some range of parameters.

Other adaptation mechanisms that have been studied do not preserve the total number of connections in the society. Jolad et al. studies networks in which connections are created

and abandoned in an attempt to achieve some preferred number of connections [45]. In this case, the adaptation mechanism reduces the expected number of contacts between the individuals as a response to the global infection prevalence, which in turn reduces the spread of infection. Zhou et al. considers growing networks in which connections between healthy and sick nodes are deleted, with the constraint that nodes can not be completely isolated [46]. In this case, the combination of network growth, connection removal, and isolation avoidance lead to recurring epidemic outbreaks. Kiss et al. studies an adaptive network in which the connections are abandoned or created at rates dependent on the status of individuals [47]. Here a variety of bifurcation structures, including bistable solutions, are observed.

We expect that in real social networks, people tend to avoid contact with their infected neighbors during an epidemic. However, once an infected neighbor recovers, people would resume social relations with that neighbor. This is in contrast to previous models in which social connections are deleted or rewired away in response to an infection, never to be resumed. In order to study this type of social behavior, we consider an adaptive network model where a susceptible node temporarily deletes or deactivates links to its infected neighbors. It then recreates or reactivates these links after its neighbors have recovered. In our model, link deletion and creation are constrained in that link creation is only allowed for the previously deleted links. There is an overarching static network structure of all possible links that could exist, and the neighborhood of each node is preserved. We assume a complex network structure rather than the complete network geometry used in [47]. Results are presented in this chapter for Erdős-Rényi random networks [48], but the approach can be used for any other complex (and potentially more realistic) network geometry. In a related model by Valdez et al., connections between susceptible and infected nodes are temporarily interrupted [49]. The period over which the connection is deactivated is shorter than the infectious period of the disease, and a connection might be interrupted and restored several times before the infected node recovered. However, because people can communicate their infection status without in-person contact (e.g., by telephone), we will assume that nodes

know the infection status of their neighbors and do not reactivate connections until their neighbors have recovered. In particular, unlike [47, 49], we do not allow links between susceptibles and infectives to be activated.

In Section 3.3, we specify the model dynamics. In Section 3.4, we present a mean field analytic approach and argue that bistability does not occur with our adaptation mechanism, in contrast to many models with rewiring adaptation. In Section 3.5, we present stochastic and mean field results for infection levels and for the geometry of the active subnetwork. We conclude and discuss future applications in Section 3.6.

3.3 Model

We study epidemic spread in a population that is represented by a network. Disease spread is modeled by using a susceptible-infected-susceptible (SIS) dynamics on the network [1]. In this model, individuals can be in one of two states: *infected* with the disease and contagious (I), or healthy and *susceptible* to the infection (S). The disease can spread via contact between susceptibles and infectives at a constant infection rate p per SI link. The infected individuals recover from the disease, becoming susceptible again, at a constant recovery rate r.

We allow healthy individuals to adapt their relationships so as to reduce the risk of being infected. In this model, susceptible individuals know the infection status of all their neighbors and can temporarily deactivate their connections to infected neighbors, a process that takes place at a deactivation rate d. Once both individuals are susceptible, the deactivated links are reactivated at a reactivation rate a. The deactivation and reactivation processes are illustrated in Fig. 3.1(a). Note that these processes take place on an unchanging network: what changes is its active part, i.e., the subset of links that allow the disease transmission.

We study the dynamics of the disease spread on a network with a fixed number of nodes, N, and a fixed number of links, K. The average degree of the network, κ, is then given by $\kappa = 2K/N$. Given an initial network geometry, the node and network dynamics

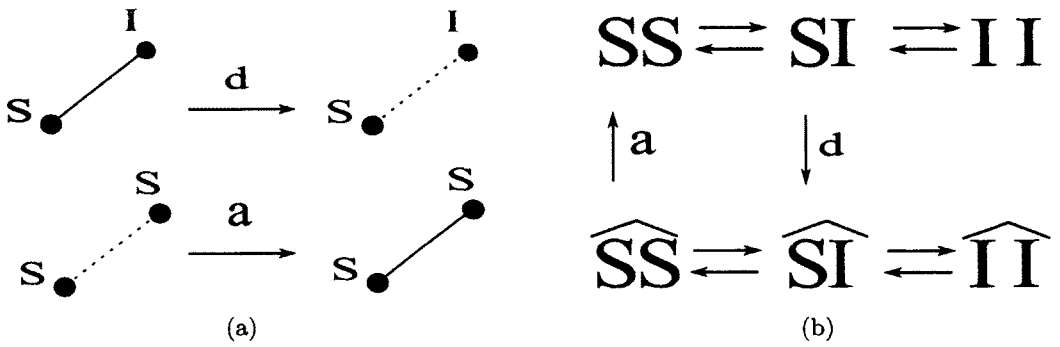

Figure 3.1: (a) Schematic of the adaptation mechanism. An active SI link is deactivated with deactivation rate d, and a deactivated SS link is reactivated with reactivation rate a. (b) Schematic of the link dynamics in the network. Horizontal arrows indicate infection (arrows toward right) and recovery (arrows toward left) transitions.

are simulated using a continuous time Monte Carlo algorithm [50]. Simulation results presented in this chapter are for Erdős-Rényi networks [48] with $N = 10^4$ and $K = 10^5$ unless otherwise specified. Self-links and multiple links between nodes are not allowed.

3.4 Analytical approach

In this section, we approximate the full system using a mean field approach [24, 7]. The following system of equations describes the evolution of the number of each type of node:

$$\frac{dN_{\mathrm{S}}}{dt} = rN_{\mathrm{I}} - pN_{\mathrm{SI}}, \tag{3.1a}$$

$$\frac{dN_{\mathrm{I}}}{dt} = -rN_{\mathrm{I}} + pN_{\mathrm{SI}}, \tag{3.1b}$$

and each type of link:

$$\frac{dN_{\mathrm{SS}}}{dt} = rN_{\mathrm{SI}} - pN_{\mathrm{SSI}} + aN_{\widehat{\mathrm{SS}}}, \tag{3.2a}$$

$$\frac{dN_{\mathrm{SI}}}{dt} = r(2N_{\mathrm{II}} - N_{\mathrm{SI}}) + p(N_{\mathrm{SSI}} - N_{\mathrm{ISI}}) - dN_{\mathrm{SI}}, \tag{3.2b}$$

$$\frac{dN_{\mathrm{II}}}{dt} = -2rN_{\mathrm{II}} + pN_{\mathrm{ISI}} \tag{3.2c}$$

$$\frac{dN_{\widehat{\mathrm{SS}}}}{dt} = rN_{\widehat{\mathrm{SI}}} - pN_{\widehat{\mathrm{SSI}}} - aN_{\widehat{\mathrm{SS}}}, \tag{3.2d}$$

$$\frac{dN_{\widehat{\mathrm{SI}}}}{dt} = r(2N_{\widehat{\mathrm{II}}} - N_{\widehat{\mathrm{SI}}}) + p(N_{\widehat{\mathrm{SSI}}} - N_{\widehat{\mathrm{ISI}}}) + dN_{\mathrm{SI}}, \tag{3.2e}$$

$$\frac{dN_{\widehat{\mathrm{II}}}}{dt} = -2rN_{\widehat{\mathrm{II}}} + pN_{\widehat{\mathrm{ISI}}}, \tag{3.2f}$$

where N_{X} denotes the expected number of nodes in state X, while N_{XY} and $N_{\widehat{\mathrm{XY}}}$ respectively denote the expected number of active and deactivated links connecting nodes in states X and Y, with X $\in$ {S,I}. The notation N_{XYZ} denotes the expected number of triples of connected nodes of type X, Y, and Z, with a circumflex over nodes that are connected by a deactivated link. Note that our definition of an XYX type of a triple includes the degenerate triples, i.e., those triples formed by a Y-node and a single X-node. Equations (3.1) reflect the transitions of nodes between susceptible and infected states, while Eqs. (3.2) reflect the link transitions indicated in Fig. 3.1(b). The values of N_{X}, N_{XY} and $N_{\widehat{\mathrm{XY}}}$ are treated as continuous in the limit of large network size.

The system of equations (3.1) and (3.2) is open since it contains unknown quantities corresponding to the statistics of the higher order node formations, i.e., the number of connected triples of nodes where at least one of the links is of SI type. Thus, in order to close the system, we approximate the number of triples in the system using the moment

closure approximation discussed in [24, 7, 25]:

$$N_{\mathrm{XSI}} = \frac{2N_{\mathrm{XS}}}{N_{\mathrm{S}}}\frac{N_{\mathrm{SI}}}{N_{\mathrm{S}}}N_{\mathrm{S}} \quad \text{for} \quad \mathrm{XS} \in \{\mathrm{SS}, \widehat{\mathrm{SS}}\} \tag{3.3a}$$

$$N_{\widehat{\mathrm{IS}}\mathrm{I}} = \frac{N_{\widehat{\mathrm{SI}}}}{N_{\mathrm{S}}}\frac{N_{\mathrm{SI}}}{N_{\mathrm{S}}}N_{\mathrm{S}} \tag{3.3b}$$

$$N_{\mathrm{ISI}} = \left(\left(\frac{N_{\mathrm{SI}}}{N_{\mathrm{S}}}\right)^2 + \frac{N_{\mathrm{SI}}}{N_{\mathrm{S}}}\right)N_{\mathrm{S}}. \tag{3.3c}$$

This closure corresponds to the assumption that, if one follows a link that stems from a susceptible node, the probability that a node at the end of that link is infected is independent of any other information available about that susceptible node.

In order to simplify the analysis, we set $r = 1$, which is equivalent to rescaling the time by $1/r$. We also rescale the quantities N_{X} and N_{XY} by N and K respectively. Since both the total number of nodes and the total number of links are conserved, the quantities $P_{\mathrm{X}} \equiv N^{-1}N_{\mathrm{X}}$ and $P_{\mathrm{XY}} \equiv K^{-1}N_{\mathrm{XY}}$ correspond to the fraction of the nodes of type X and fraction of links of type XY respectively.

Using conservation of nodes, we can eliminate one of the node equations in (3.1). Similarly, using conservation of links, we can eliminate one of the equations in (3.2). Thus, the state of the full system is approximated by the vector $\vec{x} = (P_{\mathrm{I}}, P_{\mathrm{SS}}, P_{\mathrm{SI}}, P_{\mathrm{II}}, P_{\widehat{\mathrm{SS}}}, P_{\widehat{\mathrm{SI}}})$. Note that the remaining two quantities, P_{S} and $P_{\widehat{\mathrm{II}}}$, are found from the equations for conservation of nodes and links: $P_{\mathrm{S}} = 1 - P_{\mathrm{I}}$ and $P_{\widehat{\mathrm{II}}} = 1 - P_{\mathrm{SS}} - P_{\mathrm{SI}} - P_{\mathrm{II}} - P_{\widehat{\mathrm{SS}}} - P_{\widehat{\mathrm{SI}}}$.

This system has a unique disease-free state (DFS) given by the vector $\vec{x_0} = (0, 1, 0, 0, 0, 0)$ for $a \neq 0$. We analyze the stability of the disease-free state by evaluating the Jacobian at the DFS:

$$\mathbf{J}|_{\mathbf{x_0}} = \begin{pmatrix} -1 & 0 & \frac{p\kappa}{2} & 0 & 0 & 0 \\ 0 & 0 & 1-p\kappa & 0 & a & 0 \\ 0 & 0 & -1-p-d+p\kappa & 2 & 0 & 0 \\ 0 & 0 & p & -2 & 0 & 0 \\ 0 & 0 & 0 & 0 & -a & 1 \\ 0 & -2 & d-2 & -2 & -2 & -3 \end{pmatrix}.$$

In order for the DFS to be stable, the real part of the eigenvalues of the Jacobian must be less than zero. Four of the eigenvalues of the Jacobian are $\lambda_1 = -1$, $\lambda_2 = -1$, $\lambda_3 = -2$, $\lambda_4 = -a$, all of which are less than zero. The remaining two eigenvalues λ_5 and λ_6 are given as the solutions to the equation:

$$\lambda^2 + \lambda\Big[(d+1-p\kappa)+2+p\Big] + 2(d+1-p\kappa) = 0. \tag{3.4}$$

We note that if $d+1-p\kappa > 0$ then (i) $\lambda_5\lambda_6 = 2(d+1-p\kappa) > 0$ and (ii) $\lambda_5 + \lambda_6 = -((d+1-p\kappa)+2+p) < 0$. If both (i) and (ii) hold, then both $\mathrm{Re}(\lambda_5) < 0$ and $\mathrm{Re}(\lambda_6) < 0$, and therefore the DFS must be locally stable for $p < (d+1)/\kappa$. On the other hand, the relation $\lambda_5\lambda_6 = d+1-p\kappa < 0$ implies that one of the eigenvalues is positive and the DFS loses stability. The bifurcation point

$$p^* = \frac{d+1}{\kappa}, \tag{3.5}$$

where the DFS loses stability is referred to as the *epidemic threshold.*

The non-trivial solution corresponding to the *endemic state*, $P_I > 0$, is found by setting the left hand side of equations (3.1) and (3.2) to zero. We obtain the following steady state relations for the endemic state:

$$P_{SS} = \left(\frac{d+1}{p\kappa}\right)(1-P_I), \tag{3.6a}$$

$$P_{SI} = \frac{2}{p\kappa}P_I, \tag{3.6b}$$

$$P_{II} = \frac{P_I}{\kappa} + \frac{P_I^2}{p\kappa(1-P_I)}, \tag{3.6c}$$

$$P_{\widehat{SS}} = \frac{2d}{p\kappa a}P_I, \tag{3.6d}$$

$$P_{\widehat{SI}} = \frac{2d}{p\kappa}P_I + \frac{4d}{p\kappa a}\frac{P_I^2}{1-P_I}, \tag{3.6e}$$

$$P_{\widehat{II}} = \frac{d}{p\kappa}\frac{P_I^2}{1-P_I} + \frac{2d}{p\kappa a}\frac{P_I^3}{(1-P_I)^2}. \tag{3.6f}$$

Using conservation of links, we obtain the following cubic equation in P_{I}:

$$P_{\mathrm{I}}^3 - P_{\mathrm{I}}^2(\kappa+2) + P_{\mathrm{I}}(\kappa+1+A+B) - B = 0, \tag{3.7}$$

where $A \equiv (2d)/(pa)$ and $B \equiv \kappa - (d+1)/p$. This cubic can be solved to obtain the infection level for parameter values of interest.

At the epidemic threshold, $B = 0$, Eq. (3.7) takes the form

$$P_{\mathrm{I}}\left[P_{\mathrm{I}}^2 - P_{\mathrm{I}}(\kappa+2) + \kappa + 1 + A\right] = 0.$$

Nonzero solutions are

$$P_{\mathrm{I}} = 1 + \frac{1}{2}\left(\kappa \pm \sqrt{\kappa^2 - 4A}\right), \tag{3.8}$$

both of which are either imaginary or greater than 1 for positive parameter values. Thus, at the epidemic threshold, there is no solution for $P_{\mathrm{I}} \in (0,1)$, the allowed range of endemic states. Models with rewiring adaptation typically show a backward transcritical bifurcation in the infection rate [7, 14, 11], which leads to bistability. An endemic steady state exists at the epidemic threshold in these models. We have shown that at the epidemic threshold, our model has the disease-free state as its only endemic state. We thus argue that our adaptation mechanism of link deactivation and reactivation does not produce bistability. Numerical results described in the next section support this argument and indicate that a forward transcritical bifurcation in infection rate occurs at the epidemic threshold.

Finally, we note that in the absence of adaptation, the equation below is derived by setting $a = d = 0$ and solving Eqs. (3.1) and (3.2) at the steady state:

$$P_{\mathrm{I}}^2 - P_{\mathrm{I}}(\kappa+1) + (\kappa - 1/p) = 0. \tag{3.9}$$

3.5 Results

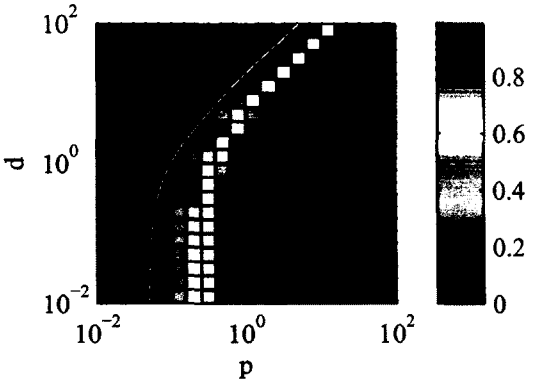

Figure 3.2: Density plot of the steady state fraction of infected nodes in the adaptive system, plotted as a function of infection rate, p, and deactivation rate, d, for the reactivation rate $a = 10$. The results of the simulations are averaged over 20 network realizations and 100 time points for each network with 1000 events between each time point. The number of events discarded as transients ranged from 3×10^9 to 10^8 for different d and p values. The white curve indicates the location of the threshold as predicted by the mean field theory in Eq. (3.5).

We next present the results of numerically simulating the adaptive system on an Erdős-Rényi random network [48] and compare the results to those predicted by the steady state of the mean field theory given by Eqs. (3.6) and (3.7). In Fig. 3.2, we show the steady state value of the fraction of infecteds as a function of infection rate p and deactivation rate d for fixed reactivation rate a. As expected, the levels of infection grow as the infection rate p is increased. Furthermore, increasing deactivation rate d leads to suppression of infection due to decreased number of potential channels of infection transmission. The onset of the endemic state is in good agreement with the mean field threshold prediction (3.5), as indicated by the white curve. We note that although Fig. 3.2 was obtained by averaging over 20 Erdős-Rényi network realizations, the standard deviation of infecteds across networks is less than 1% of the mean except very close to the threshold where variations are larger. In subsequent figures we present results for only one typical network realization, but the error bars across different realizations would generally be within the plotting resolution.

The results presented in Fig. 3.3 indicate excellent agreement of the mean field with

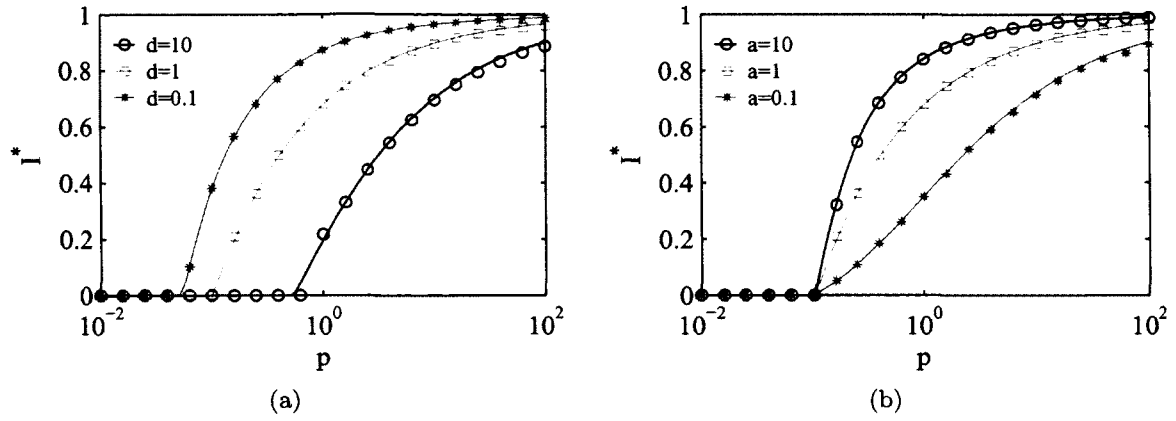

Figure 3.3: (a) Fraction of infected nodes as a function of infection rate for $a = 1$ and fixed d values. (b) Fraction of infected nodes as a function of infection rate for $d = 1$ and fixed a values. Curves are mean field solutions and symbols are simulation results. Bifurcation curves were obtained in simulations by sweeping p downward after discarding transients.

the simulations for various parameter values and demonstrate the effects of activation and deactivation on the bifurcation diagrams of fraction of infected nodes versus infection rate. Thus, in Fig. 3.3(a), we show that by varying d, we affect the location of the epidemic threshold. Note that this result is also observed in Fig. 3.2. By contrast, increasing a has no effect on the location of the epidemic threshold as shown in Fig. 3.3(b), a result that is consistent with the mean field prediction in Eq. (3.5). However, as we increase the rate of reactivation, the steady state fraction of infecteds increases, partially negating the effect of deactivation.

In our model, the initial network geometry is not evolving in time. What changes is the active part of the network, via which the disease can be transmitted. The active network geometry evolves due to the interplay between the link deactivation/reactivation and the node status. The effect that adaptation has on the network topology can be observed through the average active degree. For a given infection rate p and reactivation rate a, when the deactivation rate d is zero, the network is fully active and therefore the mean active degree simply equals the mean degree of the network. Figure 3.4 demonstrates that increasing the deactivation rate leads to the reduction of the active degree of the network and as a consequence the reduction in the expected number of infected nodes.

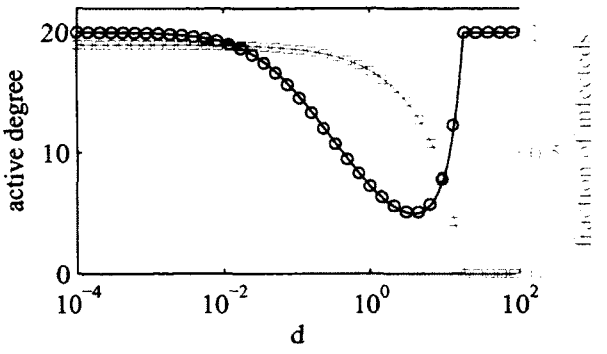

Figure 3.4: Dependence of mean active degree of the network on deactivation rate d (left axis, black circles), as compared to the dependence of the expected fraction of infected nodes on d (right axis, red squares). The solid curves are the corresponding mean field predictions and symbols are simulation results. The simulation results are obtained for $N = 10^5$, $K = 10^6$, $r = 1$, $p = 1$, $a = 10$ after discarding 10^9 number of events.

However, further increases in the deactivation rate will eventually lead to an increase in the mean active degree, while further reducing the infection level. This suggests that the adaptation mechanism functions in two qualitatively different regimes, which we attribute to the presence of slow and non-slow network dynamics regimes.

First, we consider the behavior of the system at the steady state in the limit of slow network dynamics, where deactivation and reactivation processes are much slower than the infection transmission. The steady state solution of the mean field equations (3.6) suggests that the non-trivial regime of the slow network dynamics is given by the limit of $d, a \to 0$ with $d/a = c$, for a constant c. In this limit, we study the disease spreading on a static network, frozen with only some fraction of its links being active.

The limiting behavior of our adaptive system in steady state is captured by taking the corresponding limit of the steady state solution of the mean field equations (3.6). Thus, in the limit under consideration, the terms proportional to d drop out, while the terms proportional to d/a survive, yielding the following expected fraction of deactivated and

active links in the system, respectively:

$$P^*_{\text{deactivated}} \equiv \lim_{\substack{d,a\to 0 \\ d/a=c}} \left(P_{\widehat{\text{SS}}} + P_{\widehat{\text{SI}}} + P_{\widehat{\text{II}}}\right) = \frac{2cP_{\text{I}}}{p\kappa(1-P_{\text{I}})^2}, \tag{3.10}$$

$$P^*_{\text{active}} \equiv 1 - P^*_{\text{deactivated}} = \left(1 - \frac{2cP_{\text{I}}}{p\kappa(1-P_{\text{I}})^2}\right). \tag{3.11}$$

Solving Eq. (3.11) for c and substituting the result into the corresponding limit of Eq. (3.7) (i.e., $A = 2c/p$, $B = \kappa - 1/p$), we see that P_{I} satisfies the following equation:

$$(P_{\text{I}} - 1)\left(P_{\text{I}}^2 - P_{\text{I}}\left(\kappa P^*_{\text{active}} + 1\right) + \kappa P^*_{\text{active}} - \frac{1}{p}\right) = 0.$$

Since the solution $P_{\text{I}} = 1$, where all the nodes are infected, is not a physically possible steady state, the fraction of infected nodes P_{I} must satisfy the following equation:

$$P_{\text{I}}^2 - P_{\text{I}}\left(\kappa P^*_{\text{active}} + 1\right) + \kappa P^*_{\text{active}} - \frac{1}{p} = 0, \tag{3.12}$$

which, as shown in Eq. (3.9), is precisely the equation that describes the steady state infection level in a static network with mean degree $\kappa P^*_{\text{active}}$. Note that P^*_{active} depends on all of the system parameters and the value of P_{I}, with the dependence on the deactivation and activation rates only via the ratio of those rates.

The significance of the above is that in the slow network limit, the function of adaptation is merely to suppress the mean active degree of the nodes. In other words, the adaptation reduces the mean number of potential channels for the disease transmission, regardless of the status of the nodes at the end of a channel. Figure 3.5 shows that the fraction of infected nodes in the system, when the adaptation rates are much slower than the rates of the disease dynamics, is well approximated by the mean field theory for a static network with mean degree corresponding to the mean active degree, $\kappa P^*_{\text{active}}$. Furthermore, we can see that as c approaches zero, the system approaches the mean field solution for the network without adaptation. Thus, given the active degree of the nodes in the network, possibly measured from the simulations, we can use the *static* network *mean field* description with

the corresponding mean degree (SMF) to analyze our system in this regime. Away from the limit where a and d approach zero the assumption that the disease spreads on a static network is no longer valid. In this regime the network changes on a time scale comparable to the time scale of the disease dynamics, and the nature of the adaptation mechanism becomes more complex. In Fig. 3.6, we emphasize the difference between the SMF solution and the simulation results. The overestimation of the infection levels by the static mean field approach demonstrates that, in the fast network dynamics regime, the adaptation mechanism is more effective than merely mean active degree reduction.

Now we turn to investigating how the adaptive network deviates from the static network with corresponding mean degree. Figure 3.7(a) demonstrates this deviation as we increase the adaptation parameters a and d, while keeping their ratio fixed. As we previously observed, the SMF theory makes excellent predictions about the infection levels when the network dynamics is slow; however, as the deactivation rate becomes either comparable to or greater than either the recovery or the infection rate, the SMF significantly overestimates the infection level. This is well explained by the steady state solution in Eq. (3.6), where we observe that as d is increased, the $d = 0$ assumption made when deriving the SMF is no longer valid. We quantify effects of the adaptation by looking at the local neighborhood of susceptible and infected nodes using the metric

$$\frac{\langle\kappa\rangle_{SI}}{\langle\kappa\rangle_{II}} = \frac{P_{SI}/(2P_{SS} + P_{SI})}{2P_{II}/(P_{SI} + 2P_{II})},$$

where $\langle\kappa\rangle_{SI}$ is the fraction of actively connected neighbors of a susceptible node that are infected, and similarly $\langle\kappa\rangle_{II}$ is the fraction of actively connected neighbors of an infected node that are infected. As shown in Fig. 3.7(b), at rapid deactivation rates where the SMF no longer holds, the expected fraction of infected nodes in the neighborhood of a susceptible node becomes smaller than this fraction in the neighborhood of an infected node. In other words, the mechanism of adaptation, in addition to mean degree reduction, reduces the exposure of susceptible nodes to the infected ones. The full mean field theory for the adaptive network, given by Eq. (3.7) and associated equations, continues to hold in the fast

network dynamics regime.

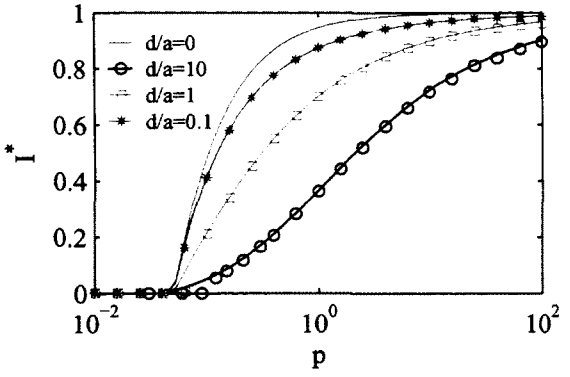

Figure 3.5: Comparison of simulation results for adaptive networks with mean field solutions for a static network (SMF), where the mean degree in the static network is matched with the active degree in the adaptive one. Curves: mean field solution of epidemic model on static network. Symbols: simulation results of epidemic model on adaptive network with $d = 10^{-2}$. Case $d/a = 0$ represents original static network with all links active. The simulation results for $d/a = 10$ and $p < 1$ are obtained for $N = 10^5$ and $K = 10^6$.

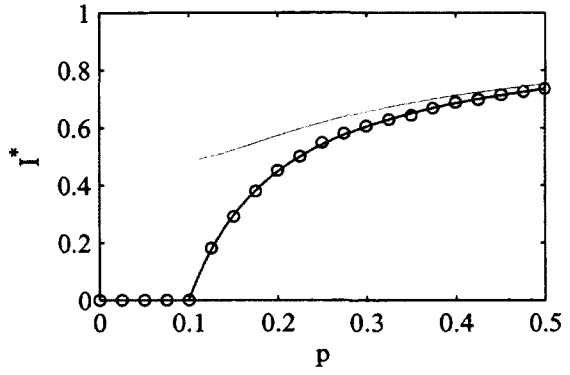

Figure 3.6: Fraction of infected nodes as a function of infection rate p in the fast adaptation regime. Black curve: mean field solution for model with adaptation. Red curve: SMF solution. Symbols: simulation results for adaptive epidemic model for $d = 1$ and $a = 10$.

3.6 Conclusions

We studied a susceptible-infected-susceptible model on an adaptive network with a new adaptation mechanism. In our model, a susceptible node temporarily deactivates its links to infected nodes. It reactivates the previously deactivated links to its neighbors once

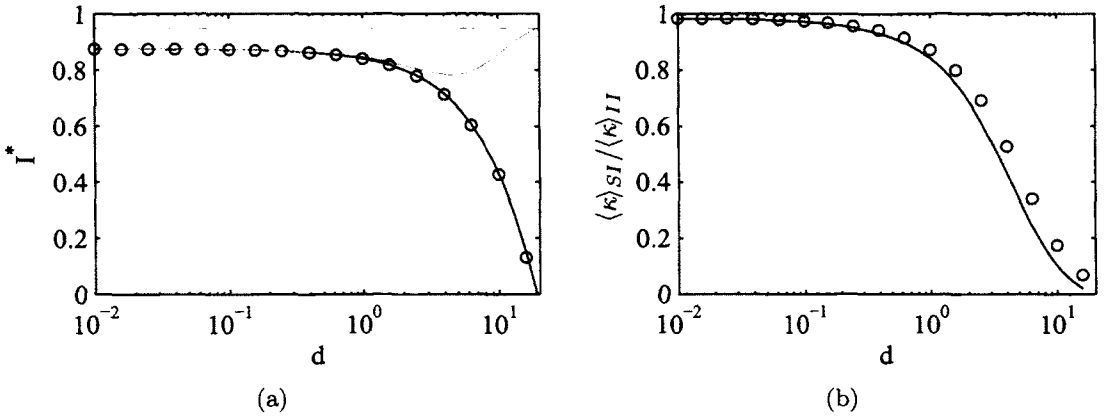

Figure 3.7: (a) Fraction of infected nodes as a function of deactivation rate d. (b) $\langle\kappa\rangle_{SI}/\langle\kappa\rangle_{II}$ as a function of d, where $\langle\kappa\rangle_{SI}$ is the fraction of infected neighbors of a susceptible node and similarly, $\langle\kappa\rangle_{II}$ is the fraction of infected neighbors of an infected node. Black solid curve: mean field solution for model with adaptation, Red solid curve: mean field solution for static model with corresponding mean degree (SMF), Red dashed curve: mean field solution for static model with all links active ($\kappa = 20$), symbols: simulation results for network with adaptation where $d/a = 0.1$ and $p = 1$.

they have recovered. Although the active degree of the node is evolving, its original set of neighbors is preserved, which we believe is a more realistic adaptation mechanism than models that allow nodes to form connections anywhere in the network.

We derived and analyzed a system of mean field equations based on a moment closure approximation. Solutions of the mean field equations were compared with simulations of the full system on an Erdős-Rényi random network and were in good agreement. An expression for the epidemic threshold was obtained. In contrast to models with a rewiring mechanism for infection avoidance [7, 14, 11, 15], our model does not display bistable solutions. We observe in numerical simulations a forward transcritical bifurcation as the infection level is increased past the threshold, and we argue from the mean field equations that a backward transcritical bifurcation and bistability cannot occur.

We studied the infection level and geometry of the active subnetwork as a function of disease and adaptation parameters. The epidemic threshold depended on the link deactivation rate but not the reactivation rate. However, slowing the reactivation decreases the steady state infection level. The average node degree in the active subnetwork was found

to depend non-monotonically on the link deactivation rate. While initially counterintuitive, this result can be understood by realizing that the epidemic is better controlled at high deactivation rates, and numbers of infectives and SI links are lower, so the total amount of link deactivation is less even though the per link deactivation rate is higher. This observation suggests that very rapid social adaptation that more effectively controls disease spread can lead to less disruption of a social network than slower adaptation would.

The adaptation mechanism in our model has two methods by which it reduces the spread of infection. Which method is most pronounced depends on the speed of the network dynamics relative to the disease dynamics. First, adaptation reduces the average active degree of the network. When deactivation and reactivation are slow, nodes change their state frequently and the infection spreads quickly on the remaining active links. The reduction in the active degree matters more than which specific links are deactivated. We compared the steady state results of our model with an SIS model on a static network having the same degree as the active degree in our model. In the regime where the dynamics of the network is much slower than the disease dynamics, the infection level in our model is very close to that in the corresponding static network. However, when both the network dynamics and the disease dynamics have comparable time scales, we observed a difference between our model and the static network model with the same active degree. Since the deactivation mechanism in our model is preferential, a susceptible node deactivates its links specifically to infected nodes. Thus, in this regime, infection spread is suppressed to a greater extent than in the corresponding static network.

In this chapter we have focused on an Erdős-Rényi random network. However, more realistic network geometries can be selected for the overarching static network. In contrast to rewiring networks, in which rewiring rules must be carefully selected to preserve desired aspects of the geometry such as community structure [42], the network structure is automatically maintained. In Chapter 4, we consider the effects of this adaptation mechanism on a scale-free network.

Another area for future study is the role of fluctuations in the different parameter

regimes. When the network dynamics is fast, a node's active degree decreases drastically while it is infected and increases while it is susceptible. However, the active degree fluctuates much less when the network dynamics are slow. Our simulations indicate that these fluctuations do not significantly affect the overall infection level in the system, but they may influence aspects of the active network geometry such as degree distributions.

Chapter 4

Epidemics with temporary link deactivation on scale-free networks

4.1 Summary

During an epidemic, people may alter their social contacts to avoid infection. Various adaptation mechanisms have been studied previously. Recently, a new adaptation mechanism was presented in [42], where susceptible nodes temporarily deactivate their links to infected neighbors and reactivate when their neighbors recover. In this chapter, we extend the temporary link deactivation mechanism to scale-free networks. We study how the topology of the active subnetwork changes in response to infection. We predict the exponent of the active degree distribution and derive mean field equations by using improved moment closure approximations based on the active degree distribution conditioned on the total degree. Our new mean field equations show better agreement with numerical simulation results compared to the standard mean field equations based on a homogeneity assumption.

The results in this chapter are in preparation to be submitted as "Epidemics with temporary link deactivation in scale free networks" by Maxim S. Shkarayev, Ilker Tunc and Leah B. Shaw. The analytical derivations in this chapter were done by Maxim S. Shkarayev.

4.2 Introduction

Many systems arising in various areas of research can be modeled as dynamical units interacting over links of a complex network, such as networks of citation in information networks; electric power line grids in technological networks; and genetic regulatory networks in biological networks [4]. Modeling spread of diseases on social networks has attracted great attention [28, 29, 4, 6, 7].

In a susceptible-infected-susceptible (SIS) dynamical model of disease, the individuals exist in one of two states: a susceptible (S), who is healthy; or an infected (I), who can transmit the disease [1]. Since disease spread is a contact process, the pattern of connections is also important to the dynamics of the disease. In compartmental models, the population is assumed to be well mixed, where every individual has a chance to contact any other [1]. The conditions under which the disease will persist and the infection level at the steady state have been well studied in these models. The assumption of homogeneous mixing is relaxed in network-based models where the pattern of contacts is represented as a network, with nodes representing individuals and links representing the social relationships between the individuals [4, 5, 6].

The complex topology of a real social network is often approximated by using simpler network models. One of the simplest is the Erdős-Rényi (ER) random graph [48], where the links are generated randomly between the nodes with a fixed probability. As a result of the random generation of links, the degree distribution is Poisson in the limit of large network size. In an ER random graph, the network geometry is characterized by the average degree of the network. Epidemic models on ER random graphs have been studied previously [24, 30]. It has been shown that there is an epidemic threshold above which the infection will persist. However, in real networks, the links are not generated randomly. In contrast there is some mechanism governing the growth of the network. Many real world networks display a power law in the tail of their degree distribution, i.e., $P(k) \sim k^{-\gamma}$, where $P(k)$ is the fraction of nodes with degree k and γ is the exponent of the distribution [5]. Networks with a power law degree distribution are called scale-free (SF) networks. In contrast to ER networks,

there is a significant probability that nodes with a large number of connected links (hubs) will exist in SF networks. It has been shown that static random SF networks do not have an epidemic threshold in the limit of large network size [28, 29, 26]. Therefore, these networks are prone to infection spreading [28, 29, 26].

In the case where the dynamics of the disease is much faster than the dynamics of the network, the network topology can be considered as static. However, during an epidemic, people may respond to the infection by changing their social contacts. Thus, the network of the social contacts may also evolve in time. Epidemic models on dynamical networks have been studied previously [46, 43, 51, 45]. If the evolution of the network depends on the state of the nodes, and the state of nodes depend on the network, then these types of networks are called adaptive networks [52].

Various adaptation rules have been considered previously. An adaptation mechanism depending on rewiring of the links is introduced in [7], where the susceptible nodes are allowed to rewire from their infected neighbors to a randomly chosen susceptible node. Here the total number of links is preserved while the links are rewired to reduce infection spread. In [14], susceptible nodes are allowed to rewire to a randomly chosen node, whereas in [15] the infected nodes are also allowed to rewire to a randomly chosen node. In [13], it is shown in simulations that rewiring leads to the same network topology independent of the initial network geometry at the steady state. In these models, the original network topology is not preserved. In some of the models, rewiring with some network structure constraints is considered. In [53], non-adaptive rewiring based on random swapping edges was introduced, where the degree distribution is preserved; in [54, 45] links are allowed to rewire adaptively while keeping the degree of the nodes. In these models, even though the original degree distribution is conserved, the original neighborhood of a node is lost. In real life, we expect that people tend to keep their connections with their friends. A new adaptation mechanism was presented in [42], based on temporary deactivation of the links with infected nodes. The deactivated links are reactivated when the infected neighbors have recovered. We studied the ER random graph as the initial network topology in Chapter 3.

In this chapter, we extend the temporary deactivation mechanism to scale-free networks. We find that adaptation changes the exponent of the degree distribution. The model based on Chapter 3 is reviewed in Section 4.3; the active degree distribution with a SF initial condition is investigated in Section 4.4. The mean field equations based on the homogeneity assumption in Chapter 3 showed good agreement with the simulations for an ER random network as we expected. However, this assumption is not valid for heterogeneous networks, such as scale-free networks. In Section 4.5, improved mean field equations are derived for the model, and show good agreement with the simulations in predicting the behavior of the inhomogeneous system.

4.3 Model

In this section, we review the model in Chapter 3. The dynamics of the disease is as follows: a susceptible node becomes infected with rate pN_{nbr}, where p is the infection rate per SI link and N_{nbr} is the number of infected neighbors of the node. An infected node becomes susceptible again with recovery rate r. As a strategy to prevent from infection, a susceptible node temporarily deactivates its links to its infected neighbors with deactivation rate d [42]. When the infected neighbor recovers, the deactivated links are reactivated with reactivation rate a. Stochastic simulations of the full system are performed by using continuous time Monte Carlo algorithm [50] on a Barabási-Albert (BA) type scale-free network [23] with total number of nodes $N = 10^5$ and fixed $r = 1$. The total degree distribution of the network is given by $P(k) = 2mk^{-3}$, where m is the minimum number of links a node has in the BA growing network algorithm [23].

4.4 Active degree distribution

The dynamics of a node's infection status depends on the number of infected nodes actively connected to it. The adaptation mechanism under consideration reduces this number by spontaneously deactivating links between susceptible and infected nodes, thus affecting

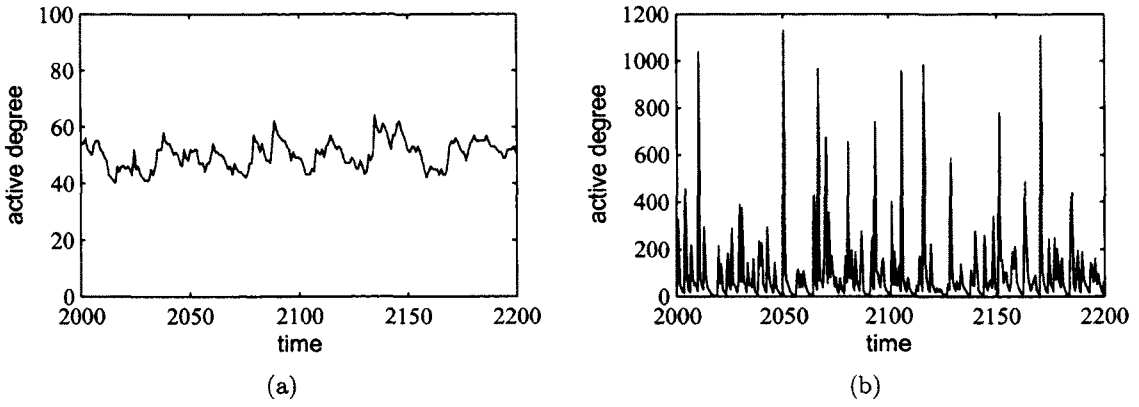

Figure 4.1: (a) Time series of the active degree of the maximum total degree node for $d/a = 1$, $d = 0.1$, $a = 0.1$ and $p = 1$. (b) Time series of the active degree of the maximum total degree node for $d/a = 1$, $d = 10$, $a = 10$ and $p = 1$. Both of the figures correspond to the same network realization, where the total degree of the node is 1268.

further disease propagation, which in turn will affect the network adaptation. Both the disease propagation and the network adaptation depend on the total number of connections a given node can have. That is, low degree nodes are less likely to have an infected node as a neighbor, which in turn means that their active degree will be less affected by the adaptation. On the other hand, nodes with a large total degree are strongly affected. In particular, those nodes are more likely to have infected neighbors and thus have their links deactivated.

The full extent of the deactivation is of particular interest when considering networks with complex topology such scale-free networks. In the following sections we show that the interplay between the disease dynamics and the adaptation leads to nontrivial changes in the topology of the active part of the network. Specifically, we show that in the network under consideration, the tail of the active degree distribution is very different from the tail of the total degree distribution. Here we present direct numerical simulations investigating the topology of the active part of the network and discuss a heuristic explanation for the observed properties of the active network topology.

4.4.1 Asymptotic nature of active degree distribution: heuristic explanation

We present a heuristic argument for the asymptotic behavior of the active degree of a node with total degree k, as a function of k. We consider the limit of $d, a \to 0$ where we expect just a few link events, i.e., events associated with link activation/deactivation, over the period of time when a given node changes its status from susceptible to infected and back to susceptible. For the slow network dynamics, the fluctuations in the active degree are expected to be less than that in the fast network dynamics. Figure 4.1 shows sample results for fixed $d/a = 1$, where the fluctuations of the active degree are much higher when $d = a = 10$. On the other hand, the fluctuations are much smaller for d and a close to zero. We argue that at the steady state we must balance the number of link events that take place while the node is in the infected state, with the number of such events while the node is in the susceptible state. We use the notation $[XY]_k$ and $[\widehat{XY}]_k$, respectively to denote the expected number of Y-nodes actively and inactively connected to an X-node with degree k. We treat these as approximately constant in the slow network limit. Thus, the average time a node spends in the susceptible state is approximated by $1/(p[SI]_k)$; in this time the expected number of deactivated links that are reactivated is given by $(a[\widehat{SS}]_k)/(p[SI]_k)$ and the expected number of links that are deactivated is given by $(d[SI]_k)/(p[SI]_k)$. On the other hand the average time interval a node spends in the infected state is $1/r$; in this time the expected number of active links that are deactivated is $(d[IS]_k)/r$. Balancing these numbers we obtain the relation:

$$\frac{1}{p[SI]_k}\left[a[\widehat{SS}]_k - d[SI]_k\right] = (d/r)[IS]_k \tag{4.1}$$

which implies that

$$[\widehat{SS}]_k = \frac{dp}{ra}[SI]_k[IS]_k + \frac{d}{a}[SI]_k \tag{4.2}$$

Let the function $f(k)$ denote the expected active degree of a node with the total degree k. With additional assumptions that $[SI]_k$ and $[IS]_k$ are proportional to $f(k)$ and assuming that $[\widehat{SS}]_k$ is proportional to the deactivated degree of a node of degree k, we get

$$k - f(k) \propto [f(k)]^2 + (r/p)f(k) \tag{4.3}$$

For high degree nodes $f(k)$ is large, so it is valid to assume that $f(k) \ll [f(k)]^2$ as the degree of the node increases. As a result, we conclude that $f(k) \propto k^{1/2}$ for large k.

The heuristic argument that we presented suggests that the tail of the active degree distribution may have different asymptotic behavior than the tail of the total degree distribution. The active degree distribution is obtained from the total degree distribution as follows:

$$P_A(A) = \sum_k P_{A|k}(A|k)P_k(k) \tag{4.4}$$

where P_k and P_A are the total and the active degree distributions respectively, while $P_{A|k}$ is the function describing the probability that a node with degree k has A active links.

In the limit where the nodes change their infection status much more frequently than links change the activity status, we assume that the conditional distribution $P_{A|k}$ is narrow and can be approximated by a delta distribution centered at the mean of $P_{A|k}$, which is equal to $f(k)$. With the additional assumption that k can be treated as continuous, the function P_A can be found by evaluating the integral

$$\begin{aligned} P_A(A) &= \int \delta\left[A - f(k)\right] P_k(k)\mathrm{d}k \qquad \text{substitute} \quad u = f(k) \\ &= \int \delta\left[A - u\right] P_k(f^{-1}(u)) \frac{1}{f'\left[f^{-1}(u)\right]}\mathrm{d}u \\ &= \frac{P_k(f^{-1}(A))}{|f'(f^{-1}(A))|} \end{aligned} \tag{4.5}$$

Using that $f(k) \sim k^{1/2}$, $f^{-1}(A) \sim A^2$, and $P_k(k) \sim k^{-3}$, we obtain $P_A(A) \sim A^{-5}$. Thus we conclude that the active degree distribution has $\sim A^{-5}$ asymptotic behavior of the tail.

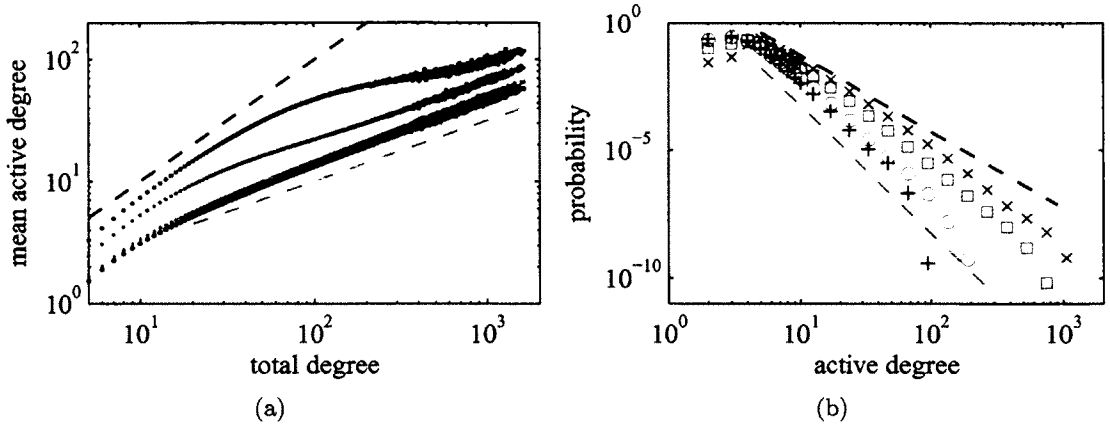

Figure 4.2: (a) Mean active degree as a function of total degree. (b) Probability distribution of active degree. In both of the figures $d/a = 1$ and $p = 1$. Black color: $d = 0.1$, red color: $d = 1$, green color: $d = 5$ and blue color: $d = 10$. In (a) red and blue dashed lines have slopes 0.5 and 1, respectively. In (b) red and blue dashed lines have slopes -5 and -3, respectively.

4.4.2 Results: Active degree distribution

We perform numerical investigation in various parameter regimes to test the results obtained using the heuristic argument. Numerical results are averaged over 100 different realizations of BA scale-free networks generated using the algorithm in [23] with $N = 10^5$ nodes and $m = 4$ (average degree 8). In each run, the results are averaged over 10^3 sample points after discarding 10^9 number of events as transients with 10^5 events between each sample. In Fig. 4.2(a) we can see that as we fix d/a and p, then for low values of d, that is whenever the network dynamics are slow, the expected active degree A as a function of the node's total degree k has a square root asymptotic dependence as predicted. As the values of d and a are simultaneously increased, and the link activity is increased, the asymptotic nature of $f(k)$ becomes less clear for the larger values of d and a. As we consider the active degree distribution, the results in Fig. 4.2(b) show that the tail of the distribution has the predicted k^{-5} asymptotic behavior for the small values of d and a. The slope of the tail deviates from -5 increasingly as the link activity is increased. Thus, we can see that the asymptotic behavior of the distribution is consistent with our prediction in the considered limit of slow network dynamics, but is inconsistent away from that limit.

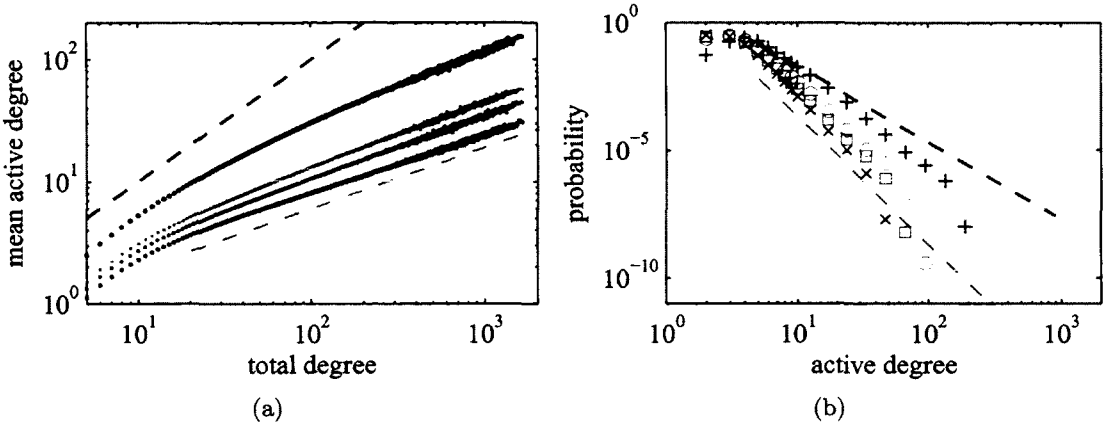

Figure 4.3: (a) Mean active degree as a function of total degree. (b) Probability distribution of active degree. In both of the figures $d = 0.1$ and $p = 1$. Black color: $d/a = 0.1$, red color: $d/a = 1$, green color: $d/a = 2$ and blue color: $d/a = 5$. In (a) red and blue dashed lines have slopes 0.5 and 1, respectively. In (b) red and blue dashed lines have slopes -5 and -3, respectively.

In Fig. 4.3 we consider the asymptotic behavior of $f(k)$ and the active degree distribution P_A as we fix d and p, while varying the value of d/a. As shown in Fig. 4.3(a), the asymptotic behavior of $f(k)$ is consistent with our $\sim k^{1/2}$ prediction, even for the large values of a (small value of d/a). As we can see from Fig. 4.3(b), while the tail of P_A appears to have the k^{-5} asymptotic behavior for small values of a, this prediction is less accurate for the large values of a, possibly due to strong link activity.

Finally, in Fig. 4.4 we consider the consistency of our prediction as we vary the values of the infection rate p. We expect our prediction about the asymptotic behavior of $f(k)$ to improve as the value of p is increased, meaning the network dynamics are slower relative to the disease dynamics, which is in fact the behavior shown in Fig. 4.4(a). Similarly, as shown in Fig. 4.4(b), the distribution P_A has $\sim k^{-5}$ asymptotic behavior for large values of p, but not for the smaller values of p, where the node activity is slow compared to the link activity.

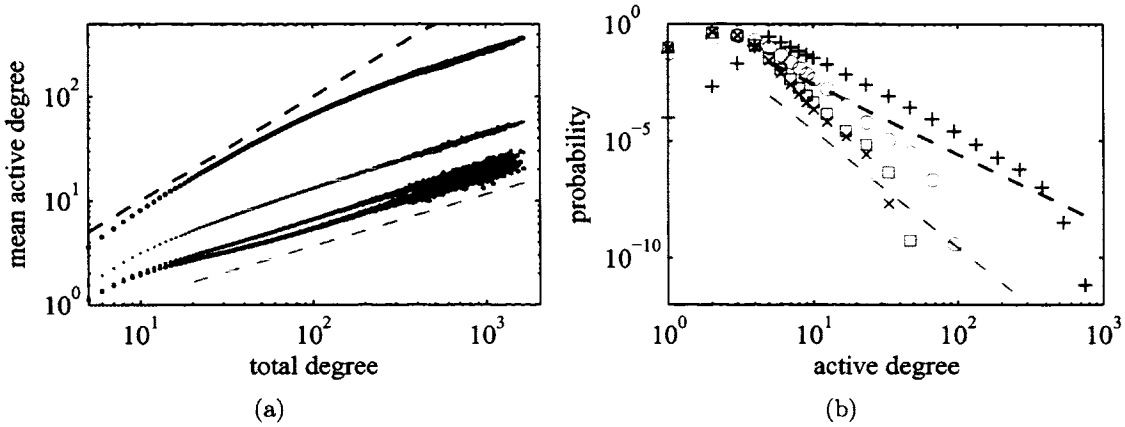

Figure 4.4: (a) Mean active degree as a function of total degree. (b) Probability distribution of active degree. In both of the figures $d = 0.1$ and $a = 0.1$. Black color: $p = 0.1$, red color: $p = 1$, green color: $p = 5$ and blue color: $p = 10$. In (a) red and blue dashed lines have slopes 0.5 and 1, respectively. In (b) red and blue dashed lines have slopes -5 and -3, respectively.

4.5 Mean field model

To analyze the full system, we need to approximate it with a lower dimensional approach. In the usual mean field approximation, nodes and links in the same state are assumed to behave similarly. Hence, the equations capturing the evolution of nodes and links are derived. Since the evolution of links (pairs) depend on higher order terms (triples), the system is open. To close the system, in moment closure approximation method, triples are derived in terms of the other variables (nodes, links) under a homogeneity assumption. In ER networks, a typical node has degree close to the average degree and the fluctuations in degree can be ignored. However, this assumption is no longer valid for networks with heterogeneous structure, such as scale-free networks where the fluctuations grow as the size of network increases. To overcome the failure of the homogeneous assumption in scale-free networks, heterogeneous mean field equations (HMF) were introduced previously [29], where the nodes are classified depending on their degrees and the system of ordinary differential equations is derived accordingly. Although these equations capture the dynamics of the system, the number of equations increases with the network size. In this section, we introduce new mean field equations based on an improved moment closure approximation derived by considering

the active degree distribution conditioned on the total degree of the nodes.

4.5.1 Moment closure approximation: beyond homogeneous closure

We review the mean field equations derived in Chapter 3. The following system of equations describes the evolution of the number of each type of node:

$$\frac{dN_{\mathrm{S}}}{dt} = rN_{\mathrm{I}} - pN_{\mathrm{SI}}, \tag{4.6a}$$

$$\frac{dN_{\mathrm{I}}}{dt} = -rN_{\mathrm{I}} + pN_{\mathrm{SI}}, \tag{4.6b}$$

and each type of link as in Chapter 3:

$$\frac{dN_{\mathrm{SS}}}{dt} = rN_{\mathrm{SI}} - pN_{\mathrm{SSI}} + aN_{\widehat{\mathrm{SS}}}, \tag{4.7a}$$

$$\frac{dN_{\mathrm{SI}}}{dt} = r(2N_{\mathrm{II}} - N_{\mathrm{SI}}) + p(N_{\mathrm{SSI}} - N_{\mathrm{ISI}}) - dN_{\mathrm{SI}}, \tag{4.7b}$$

$$\frac{dN_{\mathrm{II}}}{dt} = -2rN_{\mathrm{II}} + pN_{\mathrm{ISI}} \tag{4.7c}$$

$$\frac{dN_{\widehat{\mathrm{SS}}}}{dt} = rN_{\widehat{\mathrm{SI}}} - pN_{\widehat{\mathrm{SS}}\mathrm{I}} - aN_{\widehat{\mathrm{SS}}}, \tag{4.7d}$$

$$\frac{dN_{\widehat{\mathrm{SI}}}}{dt} = r(2N_{\widehat{\mathrm{II}}} - N_{\widehat{\mathrm{SI}}}) + p(N_{\widehat{\mathrm{SS}}\mathrm{I}} - N_{\widehat{\mathrm{I}}\mathrm{SI}}) + dN_{\mathrm{SI}}, \tag{4.7e}$$

$$\frac{dN_{\widehat{\mathrm{II}}}}{dt} = -2rN_{\widehat{\mathrm{II}}} + pN_{\widehat{\mathrm{I}}\mathrm{SI}}, \tag{4.7f}$$

where N_{X} denotes the expected number of nodes in state X, while N_{XY} ($N_{\widehat{\mathrm{XY}}}$) denote the expected number of active (deactivated) links connecting nodes in states X and Y, with $\mathrm{X} \in \{\mathrm{S},\mathrm{I}\}$. The notation N_{XYZ} denotes the expected number of triples of connected nodes of type X, Y, and Z, with a circumflex over nodes that are connected by a deactivated link. Note that our definition of an XYX type of a triple includes the degenerate triples, i.e., those triples formed by a single Y-node and an X-node. Equations (4.6) reflect the transitions of nodes between susceptible and infected states, while Eqs. (4.7) reflect the link transitions indicated in Fig. 3.1. The values of N_{X}, N_{XY} and $N_{\widehat{\mathrm{XY}}}$ are treated as continuous in the limit of large network size.

The system of equations (4.6) and (4.7) is open since it contains unknown quantities

corresponding to the statistics of higher order node formations, i.e., the number of connected triples of nodes where at least one of the links is of SI type. By definition, the triples can be found using the following equation:

$$\begin{aligned}\frac{N_{\mathrm{XSI}}}{N_S} &= \sum_{x,i} xi P_{X,I|S}(X=x, I=i|S) \quad \text{for} \quad \mathrm{XS} \in \{\mathrm{SS}, \widehat{\mathrm{SS}}\} \\ &= \sum_{x,i} xi P_{X|I,S}(x|i,S) P_{I|S}(i|S) \end{aligned} \tag{4.8}$$

where S indicates that the center node in the triple is susceptible. One way to close the system is to make an ad hoc assumption that the information about the neighborhood of a susceptible node is independent of the number of infected nodes actively connected to it. In other words, we assume that $P_{X|I,S}(x|i,S) = P_{X|S}(x|S)$, and therefore

$$\begin{aligned}\frac{N_{\mathrm{XSI}}}{N_S} &= \sum_{x,i} xi P_{X|S}(x|S) P_{I|S}(i|S) \\ &= \sum_{x} x P_{X|S}(x|S) \sum_{i} i P_{I|S}(i|S) \\ &= \frac{N_{\mathrm{SX}}}{N_S} \frac{N_{\mathrm{SI}}}{N_S} \end{aligned} \tag{4.9}$$

In the case of an ISI triple, a closure can be obtained by assuming that the distribution of infected nodes in the neighborhood of an S-node is Poisson, in which case

$$\begin{aligned}\frac{N_{\mathrm{ISI}}}{N_S} &= \sum_{i} i^2 P_{I|S}(I=i|S) \\ &= \left[\sum_{i} i P_{I|S}(I=i|S)\right]^2 + \sum_{i} i P_{I|S}(I=i|S) \\ &= \left[\frac{N_{\mathrm{SI}}}{N_S}\right]^2 + \frac{N_{\mathrm{SI}}}{N_S} \end{aligned} \tag{4.10}$$

Such an approach disregards the total degree of the node under consideration, an assumption which may be especially poor in a scale-free network, where the node degree is a highly heterogeneous quantity.

A simple way to take into account the degree of the susceptible node is to introduce additional conditioning on the total degree in Eq. (4.8):

$$\frac{N_{\mathrm{XSI}}}{N_S} = \sum_{x,i,k} xi P_{X|I,k,S}(x|i,k,S) P_{I|k,S}(i|k,S) P_{k|S}(k|S) \tag{4.11}$$

We can now close this relation by assuming that for a given degree k of the S-node, x is independent of i, i.e.,

$$P_{X|I,k,S}(x|i,k,S) = P_{X|k,S}(x|k,S), \tag{4.12}$$

then

$$\frac{N_{\mathrm{XSI}}}{N_S} = \sum_k \left[\sum_x P_{X|k,S}(x|k,S)\right] \left[\sum_i i P_{I|k,S}(i|k,S)\right] P_{k|S}(k) \tag{4.13}$$

The second assumption that we make on the way to closing the mean field system of equations is that the expected number of X-nodes in the neighborhood of an S-node is proportional to the S-node's degree k:

$$\sum_x x P_{X|k,S}(x|k,S) = C_{\mathrm{SX}}\ k \tag{4.14}$$

where the proportionality constant C_{SX} is found by averaging over the total degree k:

$$\begin{aligned} \frac{N_{\mathrm{SX}}}{N_S} &= \sum_{x,k} x P_{X|k,S}(x|k,S) P_{k|S}(k|S) = \sum_k C_{\mathrm{SX}}\ k P_{k|S}(k|S) \\ &= C_{\mathrm{SX}} \langle k \rangle_S \end{aligned} \tag{4.15}$$

Here $\langle \cdot \rangle_S$ denotes the average taken over the total degree of susceptible nodes.

As the result of the above assumptions, the expected number of triples per S-node is

found as follows:

$$\frac{N_{\mathrm{XSI}}}{N_S} = \sum_k C_{\mathrm{SI}}\, C_{\mathrm{SX}}\, k^2 P_{k|S}(k|S) = \frac{\langle k^2\rangle_S}{\langle k\rangle_S^2}\frac{N_{\mathrm{SX}}}{N_S}\frac{N_{\mathrm{SI}}}{N_S} \tag{4.16}$$

$$\frac{N_{\mathrm{ISI}}}{N_S} = \sum_k \left[C_{\mathrm{SI}}^2 k^2 + C_{\mathrm{SI}} k\right] P_{k|S}(k|S) = \left[\frac{N_{\mathrm{SI}}}{N_{\mathrm{S}}}\right]^2 \frac{\langle k^2\rangle_S}{\langle k\rangle_S^2} + \frac{N_{\mathrm{SI}}}{N_{\mathrm{S}}} \tag{4.17}$$

In order to complete the closure, we must estimate the values of the ratio $\alpha \equiv \langle k^2\rangle_S/\langle k\rangle_S^2$. We present the estimate of these moments in the two limits: near bifurcation and in the limit of strong infection p.

Our numerical simulations allow us to conclude that the solution undergoes a transcritical bifurcation at the threshold value in the case of finite size networks. Therefore, in the limit as p approaches the threshold from above, the expected number of infected nodes approaches zero, and as a result in this limit the degree distribution of susceptible nodes must approach the network's total degree distribution $P_k(k) = 2m^2k^{-3}$. In this case the value of α will depend on the size of the network, and will approach infinity in the limit of infinite network size.

In order to estimate α in the limit of large values of p, we consider the following relation:

$$P_{k|S}(k|S) = P_{S|k}(S|k)\frac{P_k(k)}{P_S(S)} \tag{4.18}$$

where the probability that the degree of a randomly chosen node is k is given by the total degree distribution, $P_k(k)$, and the probability, $P_S(S)$, that a randomly chosen node is susceptible given by $N_S/(N_S + N_I)$, i.e., is the fraction of susceptible nodes in the system. Function $P_{S|k}(S|k)$ is the probability that a node with total degree k is susceptible. We approximate its value by estimating the fraction of time a node with degree k spends in a

susceptible state:

$$P_{S|k}(S|k) = \frac{\frac{1}{p[SI]_k/[S]_k}}{1/r + 1/(p[SI]_k/[S]_k)} = \frac{1}{(p/r)[SI]_k/[S]_k + 1} \propto ([SI]_k/[S]_k)^{-1} \quad \text{in the limit of large} \quad p \tag{4.19}$$

where $1/(p[SI]_k/[S]_k)$ is the expected amount of time it takes for an S-node with $[SI]_k/[S]_k$ infected neighbors to be infected, and $1/r$ is the expected amount of time it takes an infected node to recover. In the limit of large p we obtain:

$$P_{k|S}(k|S) \sim ([SI]_k/[S]_k)^{-1} P_k(k) \sim k^{-1} P_k(k) \tag{4.20}$$

Using $P_k(k) \sim k^{-3}$ for BA scale-free network, we get

$$P_S(k) \sim k^{-4} = ck^{-4} \quad \text{for some constant} \quad c \tag{4.21}$$

Then treating k as continuous

$$\int_{k_{min}=m}^{\infty} ck^{-4} dk = 1 \quad \Rightarrow \quad c = 3m^3 \tag{4.22}$$

Using Eq. (4.22) we get:

$$\frac{\langle k^2 \rangle_S}{\langle k \rangle_S^2} = \frac{\int_m^{\infty} k^2 P_S(k) dk}{\left[\int_m^{\infty} k P_S(k) dk\right]^2} = \frac{4}{3} \quad \text{for} \quad m = 10. \tag{4.23}$$

4.5.2 Results: Mean field

In Figs. 4.5 we present the results of simulating the spread of disease on a realization of the scale-free network generated according to the algorithm in [23] for $m = 10$. To locate the

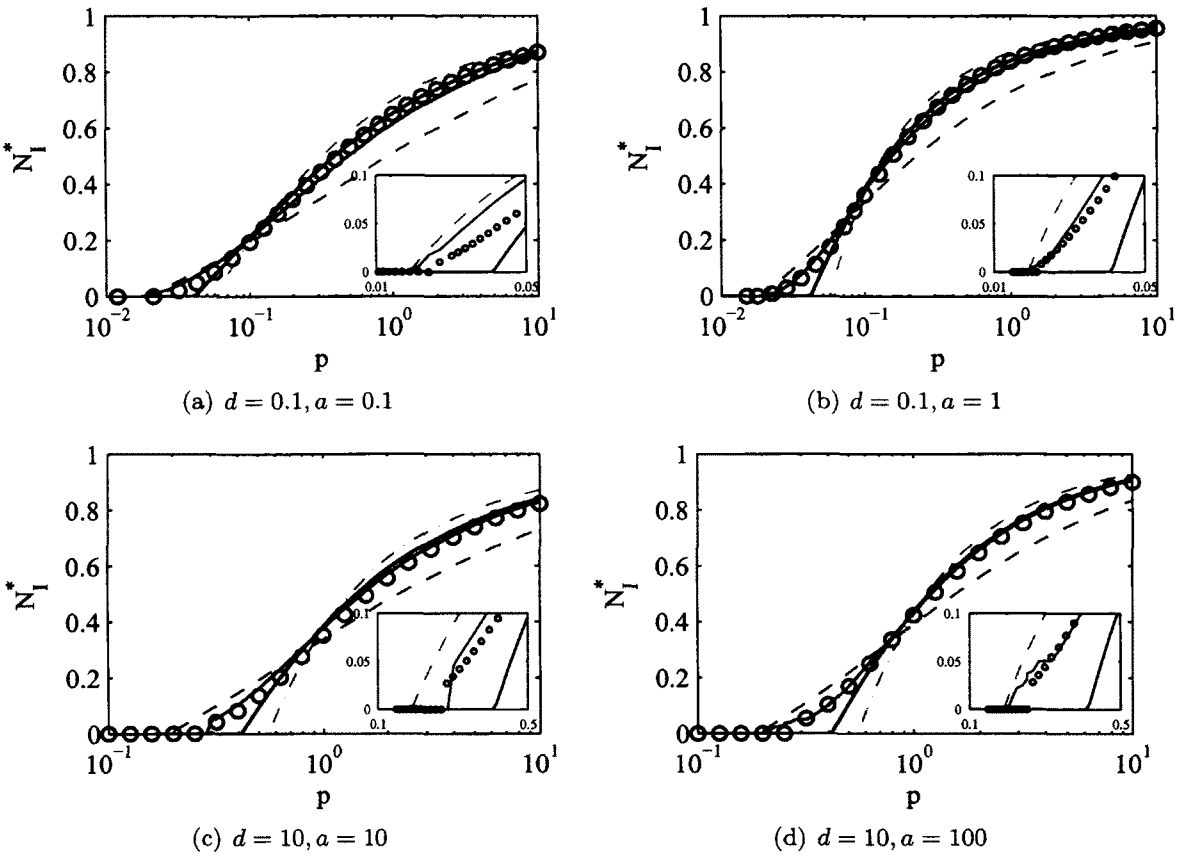

(a) $d = 0.1, a = 0.1$

(b) $d = 0.1, a = 1$

(c) $d = 10, a = 10$

(d) $d = 10, a = 100$

Figure 4.5: Steady state fraction of infecteds as a function of infection rate p for different d and a values. Circles: simulation results; red dot-dashed curve: solutions of the standard mean field equations; green dashed curve: solutions of the mean field equations closed using closure A (near bifurcation); black solid curve: solutions of the mean field equations closed using closure B (limit of large p); blue solid curve: solutions of the mean field equations closed using closure C (using simulations).

endemic branch, we first simulated the system for a long time for $p = 10$. Then p values are swept from $p = 10$ to lower ones. The steady state infection level for each p value is obtained using the sampling described in Section 4.4.2. The final state of each run is used as an initial state for the next p value. The results of the direct simulations are compared to the mean field approximation found in Eqs. (4.6)-(4.7), which were closed using two different assumptions: firstly, infected nodes are distributed homogeneously in the neighborhood of susceptible nodes as in Eqs. (4.9)-(4.10), and secondly, the distribution of the infected nodes is homogeneous when conditioned on the total degree of the susceptible nodes. The second

closure is completed by

- closure A: approximating the value of α with that for the total degree distribution for all the nodes, which is only expected to perform well near the threshold where almost all of the nodes are expected to be susceptible ($\alpha = 2.9$).
- closure B: with the expression derived in Eq. (4.23) for the large infection rate limit
- closure C: using the value of α measured directly from the simulations.

As we can see from Fig. 4.5, the usual moment closure based on homogeneity rarely performs well, since it is equivalent to the closure B with an assumption that $P_S(k)$ is given by the delta function, as that is the only distribution for which $\alpha = 1$. Such an assumption performs particularly poorly for the scale-free network.

Closure C performs well everywhere, suggesting that the homogeneity assumption with the total degree conditioning is a good approximation. However, this approach is limited as it is based on the information obtained from the simulations and cannot be used for analytical study of the system. The two remaining closures perform well in their respective derivation limits. Thus, closure B shows excellent agreement with the simulations except near the epidemic threshold. On the other hand, closure A is the most accurate in its prediction of the threshold location, which appears to be nonzero for the finite network size.

Thus, we conclude that the approximation in Eq. (4.12) is a minor source of error and completing the closure relies heavily on how well we can approximate the value of α for a broad range of parameters.

4.6 Conclusions

We extended the adaptation mechanism based on the temporary deactivation/reactivation of links [42] to scale-free networks. Although the topology of the original network is not changing, the active subnetwork is dynamic under this adaptation mechanism. We studied how the active degree distribution of the network evolves as the disease spreads in the

network. We observed that the active degree distribution is a power law with a different exponent than the original degree distribution of the network. A heuristic argument explaining that observation is presented. The heuristic argument shows that nodes with different total degree are affected disproportionately under the adaptation mechanism. By using that heuristic argument, the exponent of the active degree distribution is predicted. We observe that the predicted exponent of the tail of the active degree distribution shows good agreement with the simulation results in the limit when network dynamics is slow relative to disease dynamics.

In order to derive mean field equations for the full system, we improved the commonly used homogeneous moment closure approximation. The moment closure approximation in previous studies is based on the assumption that infected and susceptible neighbors of a susceptible node are independent of each other and independent of node degree. This assumption is more valid for a random network where the distribution of the neighbors of a susceptible node is Poisson. In order to improve that approximation, we take into account the active degree distribution conditioned on total degree, and we obtain a closure with an additional factor depending on the degree distributionof susceptible nodes. We approximated analytically the value of this factor in two different regions. Direct numerical simulations of the full network system indicate that the system undergoes a forward bifurcation where the disease free state loses stability. In the region where the system is near the bifurcation, we assumed that the degree distribution of susceptibles is close to the degree distribution of the original network. Therefore, we were able to predict the factor approximately. On the hand, in the region where infection rate p is large, we were also able to predict the factor. Our improved mean field showed better agreement with simulation than the homogeneous mean field in both of these regions. For other values of infection rate p, we directly find the factor from the simulations, and the results of the mean field equations showed good agreement for these p values.

Chapter 5

Conclusions

In this dissertation, we studied the effects of network structure on epidemic spreading in adaptive social networks. The spread of an epidemic in a population is strongly related to the structure of the underlying network of social contacts. Therefore, it is crucial to understand the interplay between the structure of the population and the dynamics of the disease in order to better understand and prevent the spread of a disease. Moreover, individuals may respond to infection by changing their connections. Thus, the geometry of the network becomes a dynamic process. It is also important to understand the effects of the local rules determined by the behaviors of individuals on the epidemic spread in order to design methods to prevent the spread of the disease in the large scale population. We contributed to research in this area by studying the role of community structure in adaptive networks. Moreover, we introduced a new adaptation strategy more realistic than the previous models based on random link rewiring [7, 11, 14, 15], and we studied the effects of this adaptation strategy on the epidemic spread. In addition, we analyzed the geometry of the active subnetwork for ER random graphs and BA scale-free networks.

In Chapter 2, we studied a susceptible-infected-susceptible (SIS) model on an adaptive network having two connected heterogeneous communities. The heterogeneity between the two networks is represented by different average degrees. Moreover, we considered different network topologies by tuning a coupling strength parameter, which determines the number

of links between the two communities. In particular, we studied cases with strong coupling and weak coupling. A rewiring adaptation mechanism similar to [7] is used, but it is modified so that the initial network geometry with community structure is preserved if the links to be rewired are randomly distributed. In the absence of rewiring, low infection level in the subthreshold community and high infection level in the higher average degree community are observed. Stochastic reintroduction of infection due to the connection to a high infection level community is observed in the subthreshold community. However, when the coupling strength is increased, both of the networks behaved similarly. For the adaptive case, whether the communities are strongly or weakly coupled, they behave similarly in terms of infection levels at the steady state. In the case of weakly coupled communities, there is a very slow process that synchronizes the average degrees of the two communities. We analyzed the two community adaptive network system by deriving mean field equations, and the results showed good agreement with the simulations at the steady state. We showed that the adaptation mechanism changes the network structure such that both of the communities becomes similar in average degree.

In Chapter 3, we introduced a new adaptation strategy that is more realistic than the rewiring mechanism. In our temporary deactivation mechanism, a susceptible node temporary deactivates its links to its infected neighbors instead of rewiring. Once a neighbor recovers, the deactivated link with that neighbor is reactivated again. In contrast to previous rewiring models, the original neighborhood of a node is preserved. Even though the original network is static, the active subnetwork is evolving in time.

We demonstrated that the effect of the adaptation is mainly to decrease the average degree of the network when network dynamics is slower than the disease dynamics. In this regime, the system behaves similar to a static network with an average degree the same as the active degree of the adaptive network. However, for the case where the network dynamics is fast, we observed that the adaptation mechanism further suppresses the infection by reducing the dangerous links to infected nodes.

In Chapter 3, we considered an Erdős Rényi (ER) random graph as the original network.

The degree distribution of an ER random graph is Poisson in the limit of large network size. However, many real world networks are scale-free, where the degree distribution follows a power law. In Chapter 4, we extended the adaptation with link deactivation to scale-free networks.

We studied the effects of the epidemic spread on the geometry of the active subnetwork, where the original network is a BA scale-free network with exponent -3. We showed that the link deactivation mechanism changes the exponent of the distribution. We predicted the exponent of the tail of the active degree distribution. The standard mean field equations based on the homogeneity assumption fail to predict the behavior of the system for scale-free networks. We obtained improved mean field equations based on a new moment closure approximation, which is derived by considering the active degree distribution conditioned on the total degree. The new closure has an additional factor depending on the active degree distribution of susceptible nodes. In the limit of large infection rate and near the epidemic threshold, we were able to predict that factor analytically. For the general case, the factor was directly calculated from simulations. The new mean field approach showed better agreement with the simulations compared to the standard mean field equations.

As future extensions to this work, the models we studied in this dissertation can be applied to more realistic adaptive network structures. In Chapter 2, we studied epidemic spread on an adaptive network having two communities with rewiring adaptation. More realistically, the temporary deactivation mechanism can be considered on a network having multiple connected communities. In Chapter 4, we were able to show that the deactivation mechanism changes the tail of the distribution for the BA scale-free networks. This work can be extended to include more general scale-free networks with exponents other than -3.

Bibliography

[1] R.M. Anderson, R.M. May, *Infectious Diseases of Humans: Dynamics and Control* (Oxford University Press, Oxford, 1992)

[2] F. Brauer, P. Van den Driessche, J. Wu, *Lecture Notes in Mathematical Epidemiology* (Springer, 2008)

[3] S.N. Dorogovtsev, J. Mendes, Adv. Phys. **51**(4), 1079 (2002)

[4] M.E.J. Newman, SIAM review **45**(2), 167 (2003)

[5] R. Albert, A.L. Barabási, Reviews of modern physics **74**(1), 47 (2002)

[6] M. Keeling, K. Eames, Journal of the Royal Society Interface **2**(4), 295 (2005)

[7] T. Gross, C.J.D. D'Lima, B. Blasius, Physical Review Letters **96** (2006)

[8] T. Gross, B. Blasius, Journal of the Royal Society Interface **5**(20), 259 (2008)

[9] I.B. Schwartz, L.B. Shaw, Physics **3**, 17 (2010)

[10] X. Tan, S. Li, C. Wang, X. Chen, X. Wu, Health Education Research **19**(5), 576 (2004)

[11] L.B. Shaw, I.B. Schwartz, Physical Review E **77**(6), 066101 (2008)

[12] S. Van Segbroeck, F.C. Santos, J.M. Pacheco, PLoS Comput. Biol. **6**(8), e1000895 (2010). DOI 10.1371/journal.pcbi.1000895

[13] V. Marceau, P. Noël, L. Hébert-Dufresne, A. Allard, L. Dubé, Physical Review E **82**(3), 036116 (2010)

[14] D. Zanette, S. Risau-Gusmán, J. Biol. Phys. **34**(1), 135 (2008)

[15] S. Risau-Gusmán, D. Zanette, Journal of theoretical biology **257**(1), 52 (2009)

[16] M.E.J. Newman, M. Girvan, Physical Review E **69**(2), 026113 (2004)

[17] S. Boccaletti, V. Latora, Y. Moreno, M. Chavez, Physics reports **424**, 175 (2006)

[18] P. Erdos, Acta Mathematica Hungarica (1961)

[19] M. Newman, *Networks: An Introduction* (Oxford University Press, Inc., New York, NY, USA, 2010)

[20] R. Albert, H. Jeong, A.L. Barabási, Nature **401**(6749), 130 (1999)

[21] M. Faloutsos, P. Faloutsos, C. Faloutsos, in *Proceedings of the conference on Applications, technologies, architectures, and protocols for computer communication, SIGCOMM '99*, vol. 29 (ACM, 1999), *SIGCOMM '99*, vol. 29, pp. 251–262

[22] H. Jeong, B. Tombor, R. Albert, Z.N. Oltvai, A.L. Barabasi, Nature **407**(6804), 651 (2000)

[23] A.L. Barabási, R. Albert, Science **286**(5439), 509 (1999)

[24] M.J. Keeling, D.A. Rand, A.J. Morris, Proc. R. Soc. Lond. B **264**(1385), 1149 (1997)

[25] M.S. Shkarayev, I.B. Schwartz, L.B. Shaw, arXiv:1111.0964 (2012)

[26] R. Pastor-Satorras, A. Vespignani, Physical Review E **63**, 066117 (2001)

[27] M. Kuperman, G. Abramson, Physical Review Letters **86**(13), 2909 (2001). DOI 10.1103/PhysRevLett.86.2909

[28] R.M. May, A. Lloyd, Physical Review E **64**(6), 066112 (2001)

[29] R. Pastor-Satorras, A. Vespignani, Physical Review Letters **86**(14), 3200 (2001)

[30] M.E.J. Newman, Physical Review E **66**(1), 016128 (2002)

[31] G. Yan, Z.Q. Fu, J. Ren, W.X. Wang, Physical Review E **75**(1), 016108 (2007)

[32] W. Huang, C. Li, J. Stat. Mech: Theory Exp. **2007**(01), P01014 (2007)

[33] X. Chu, J. Guan, Z. Zhang, S. Zhou, J. Stat. Mech: Theory Exp. **2009**(07), P07043 (2009). DOI 10.1088/1742-5468/2009/07/P07043

[34] H. Zhao, Z.Y. Gao, Europhys. Lett. **79**(3), 38002 (2007)

[35] Z. Liu, B. Hu, Europhys. Lett. **72**(2), 315 (2005)

[36] J. Zhou, Z. Liu, Physica A **388**(7), 1228 (2009). DOI 10.1016/j.physa.2008.12.014

[37] C. Xia, S. Sun, F. Rao, J. Sun, J. Wang, Z. Chen, Front. Comput. Sci. China **3**(3), 361 (2009)

[38] H. Sun, Z. Gao, Physica A **381**, 491 (2007). DOI 10.1016/j.physa.2007.03.030

[39] B. Wang, L. Cao, H. Suzuki, K. Aihara, J. Phys. A: Math. Theor. **44**(3), 035101 (2011). DOI 10.1088/1751-8113/44/3/035101

[40] D.T. Gillespie, J. Comput. Phys. **22**(4), 403 (1976). DOI 10.1016/0021-9991(76)90041-

[41] B. Ermentrout, Simulating, Analyzing, and Animating Dynamical Systems A Guide to XPPAUT for Researchers and Students 1st ed. Philadelphia, PA: SIAM (2002)

[42] I. Tunc, M.S. Shkarayev, L.B. Shaw, Journal of Statistical Physics pp. 1–12 (2012). DOI 10.1007/s10955-012-0667-7

[43] Y. Schwarzkopf, A. Rákos, D. Mukamel, Physical Review E **82**(3), 036112 (2010)

[44] M. Taylor, T. Taylor, I. Kiss, Physical Review E **85**(1), 016103 (2012)

[45] S. Jolad, W. Liu, B. Schmittmann, R.K.P. Zia, arXiv:1109.5440v1 (2011)

[46] J. Zhou, G. Xiao, S. Cheong, X. Fu, L. Wong, arXiv:1203.0366v1 pp. 1–8 (2012)

[47] I.Z. Kiss, L. Berthouze, T.J. Taylor, P.L. Simon, Proceedings of the Royal Society A: Mathematical, Physical and Engineering Sciences **468**(2141), 1332 (2012)

[48] P. Erdős, A. Rényi, Publicationes Mathematicae Debrecen **6**, 290 (1959)

[49] L.D. Valdez, P.A. Macri, L.A. Braunstein, Physical Review E **85**, 036108 (2012)

[50] D.T. Gillespie, J. Phys. Chem **81**(25), 2340 (1977)

[51] G. Demirel, T. Gross, arXiv preprint arXiv:1209.2541 (2012)

[52] T. Gross, I.G. Kevrekidis, Europhys. Lett. **82**(3), 38004 (2008). DOI 10.1209/0295-5075/82/38004

[53] E. Volz, L.A. Meyers, Proceedings of the Royal Society B: Biological Sciences **274**(1628), 2925 (2007)

[54] J. Yoo, J. Lee, B. Kahng, Physica A: Statistical Mechanics and its Applications **390**(23), 4571 (2011)

Vita

Ilker Tunc was born in Samsun, Turkey. He graduated from Middle East Technical University with a Bachelors of Science degree in Mathematics Education in June, 2000. He has a Masters of Science degree in Mathematics from Istanbul Technical University. In 2008, he started his Ph.D. education on Mathematical and Computational Biology in Applied Science Department.